UvA-DARE (Digital Academic Repository)

Higher Order Visual Areas Enhance Stimulus Responsiveness in Mouse Primary Visual Cortex

Oude Lohuis, M.N.; Cervan Canton, A. ; Pennartz, C.M.A.; Olcese, U.

Citation for published version (APA):
Oude Lohuis, M. N., Cervan Canton, A., Pennartz, C. M. A., & Olcese, U. (2022). Higher Order Visual Areas Enhance Stimulus Responsiveness in Mouse Primary Visual Cortex. *Cerebral Cortex*, *32*(15), 3269-3288. https://doi.org/10.1093/cercor/bhab414

Higher order visual areas enhance stimulus responsiveness in mouse primary visual cortex

Matthijs N. Oude Lohuis[1,2], Alexis Cervan Canton[1,3], Cyriel M. A. Pennartz[1,2], Umberto Olcese[1,2]

[1]Cognitive and Systems Neuroscience Group, Swammerdam Institute for Life Sciences, University of Amsterdam, 1098XH Amsterdam, The Netherlands,
[2]Amsterdam Brain and Cognition, University of Amsterdam, 1098XH Amsterdam, The Netherlands,
[3]Current address: Institut d'Investigacions Biomèdiques August Pi i Sunyer (IDIBAPS), 08036 Barcelona, Spain

*Address correspondence to Umberto Olcese, Cognitive and Systems Neuroscience Group, Swammerdam Institute for Life Sciences, University of Amsterdam, Science Park 904, 1098XH Amsterdam, The Netherlands. Email: u.olcese@uva.nl

Over the past few years, the various areas that surround the primary visual cortex (V1) in the mouse have been associated with many functions, ranging from higher order visual processing to decision-making. Recently, some studies have shown that higher order visual areas influence the activity of the primary visual cortex, refining its processing capabilities. Here, we studied how in vivo optogenetic inactivation of two higher order visual areas with different functional properties affects responses evoked by moving bars in the primary visual cortex. In contrast with the prevailing view, our results demonstrate that distinct higher order visual areas similarly modulate early visual processing. In particular, these areas enhance stimulus responsiveness in the primary visual cortex, by more strongly amplifying weaker compared with stronger sensory-evoked responses (for instance specifically amplifying responses to stimuli not moving along the direction preferred by individual neurons) and by facilitating responses to stimuli entering the receptive field of single neurons. Such enhancement, however, comes at the expense of orientation and direction selectivity, which increased when the selected higher order visual areas were inactivated. Thus, feedback from higher order visual areas selectively amplifies weak sensory-evoked V1 responses, which may enable more robust processing of visual stimuli.

Key words: brain state; higher order visual areas; orientation selectivity; top-down modulation; visual processing.

Introduction

The various areas which make up the mouse visual cortical system have, over the past decade, emerged as a prime model to study the functional architecture underlying vision in mammals (Wang and Burkhalter 2007; Andermann et al. 2011; Marshel et al. 2011; Glickfeld et al. 2014; Glickfeld and Olsen 2017). The anterior and lateral borders of primary visual cortex V1 are surrounded by an array of areas, collectively called higher order visual areas (HVAs), each having distinct connectivity patterns and visual response properties, and providing a specific contribution to visual processing (Andermann et al. 2011; Marshel et al. 2011; Wang et al. 2012). Several studies have investigated what functions each of these areas might fulfill in visual processing. A wide range of functions has been found, complementing V1 in orientation discrimination and contrast detection (Jin and Glickfeld 2020), spatial integration (Murgas et al. 2020), perception of higher order visual features (Khastkhodaei et al. 2016), and illusory contours (Pak et al. 2020). Furthermore, HVAs partially overlap with the rodent posterior parietal cortex and have been implicated in several functions beyond simple visual processing, for instance multisensory integration (Olcese et al. 2013; Song et al. 2017; Meijer et al. 2020), (multi)sensory evidence accumulation and decision-making (Raposo et al. 2014; Erlich et al. 2015; Hanks et al. 2015; Licata et al. 2017), and navigation (Harvey et al. 2012; Krumin et al. 2018). Moreover, HVAs play a significant role in sensory processing by means of the input they provide not only to each other but also to V1 (Wang et al. 2012).

Feedback projections from HVAs to V1 have been found to be functionally organized (Kim et al. 2018; Marques et al. 2018), similarly to local connections (Ko et al. 2011; Cossell et al. 2015) and feedforward projections from V1 to HVAs (Berezovskii et al. 2011; Glickfeld et al. 2013). These feedback projections have been associated with a variety of essential forms of visual processing: response facilitation (Pafundo et al. 2016; Nurminen et al. 2018), surround suppression (Nassi et al. 2013;

Nurminen et al. 2018; Vangeneugden et al. 2019), and predictive processing (Keller et al. 2020). A recent study, in particular, showed that each HVA differently impacts the activity of V1 neurons based on their visual response properties (Huh et al. 2018). Inactivating either the anterolateral (AL) or posteromedial (PM) area primarily reduced the responses of those V1 neurons showing functional properties similar to those of AL and PM, respectively. The Huh et al. (2018) study focused on tuning of V1 cells to spatial frequency and investigated how inactivating AL and PM modulates firing rate responses to drifting gratings moving along the preferred orientation of single neurons. Overall, previous studies thus indicate that feedback projections from HVAs to V1 may provide a mechanism to enhance the processing of specific visual stimuli, based on the response properties of each HVA. We expanded the results of previous literature by combining optogenetics and ensemble recordings to investigate how HVAs contribute to a broad spectrum of V1 functions—such as orientation and direction selectivity, receptive field size, and single-trial encoding of visual features—as a function of the speed of visual stimuli. We further compared anesthetized and awake conditions. Unconscious brain states have been associated with lacking or diminished recurrent processing (Lamme et al. 1998; Makino and Komiyama 2015; Keller et al. 2020) and we investigated whether functionally specific feedback is degraded under anesthetized conditions. Surprisingly, we found that, in addition to the previously reported, functionally specific feedback (in which modulation of V1 varies based on the functional tuning of each HVA), AL and PM similarly enhance V1 responsiveness to visual stimuli, during both wakefulness and anesthesia. Such enhancement is especially prominent for weak sensory-evoked responses and for responses entering the receptive field of single neurons but comes at the expense of orientation and direction selectivity. Thus, in addition to previously discovered functions, HVAs also contribute to amplifying V1 responses, especially to stimuli which would otherwise evoke small changes in spiking activity.

Materials and Methods
Subjects

All animal experiments were performed according to the national and institutional regulations. The experimental protocol was approved by the Dutch Commission for Animal Experiments and by the Animal Welfare Body of the University of Amsterdam. A total of 14 male mice from two transgenic mouse lines were used: PVcre (B6;129P2-Pvalbtm1(cre)Arbr/J, JAX mouse number 008069) and F1 offspring of this same PVcre line with Ai9-TdTomato cre reporter mice (B6.Cg-Gt(ROSA)26Sor$^{tm9(CAG-tdTomato)Hze}$/J, JAX mouse number 007909). Animals were at least 8 weeks of age at the start of experiments. Mice were group housed, with ad libitum access to water and food, under a reversed day–night schedule (lights

were switched off at 8:00 and back on at 20:00). All experimental procedures were performed during the dark period.

Experimental Design
Headbar Implantation

Mice were subcutaneously injected with the analgesic buprenorphine (0.025 mg/kg) and maintained under isoflurane anesthesia (induction at 3%, maintenance at 1.5–2%) during surgery. The skin above the skull was epilated, disinfected, and a circular area was removed with the edges glued to the outer parts of the skull using tissue adhesive (3-M Vetbond) to prevent postsurgical infections. A custom-made titanium head-bar with a circular recording chamber (inner diameter: 5 mm) was positioned over the exposed skull of the left hemisphere to include visual, auditory, and somatosensory cortices and attached using cyanoacrylate and C&B Super-Bond (Sun Medical).

Intrinsic Optical Imaging

To localize individual higher visual cortical areas, we performed intrinsic optical imaging (IOI) under lightly anesthetized conditions (0.7–1.2% isoflurane). A vasculature image was acquired under 540-nm light before starting the imaging session. During IOI, the cortex was illuminated with monochromatic 630-nm light. Images were acquired at 1 Hz using an Adimec 1000-m CCD camera (1004 × 1004 pixels) connected to a frame grabber (Imager 3001, Optical Imaging Inc.), defocused ~500–600 μm below the pial surface.

We presented visual, auditory, and tactile stimuli. Visual stimuli consisted of full field drifting gratings (spatial frequency 0.05 cpd, temporal frequency 1.5 Hz) for 1 s in each of eight directions. Auditory stimuli consisted of alternations between chirps sweeping up or down in frequency (1–40 kHz) and band-passed white-noise (1–40 kHz) calibrated at 70-dB Sound Pressure Level. Tactile stimuli were full whisker-pad deflections driven by a piezo-actuator (18° angle). For each type of stimulation, we acquired 8 s of baseline signal and 8 s of hemodynamic response during stimulation. The acquired frames during the response were baseline-subtracted, averaged, and thresholded to produce a map of localized individual primary and higher order areas. PM and AL were identified based on the IOI signal map in combination with previously published maps (Wang and Burkhalter 2007; Olcese et al. 2013; Glickfeld and Olsen 2017) and marked on the skull based on the vasculature image. After IOI, the recording chamber was covered with silicon elastomer (Picodent Twinsil) and mice were allowed to recover for 2–7 days.

Viral Injections

Mice were subcutaneously injected with the analgesic buprenorphine (0.025 mg/kg) and maintained under isoflurane anesthesia (induction at 3%, maintenance at 1.5–2%) during surgery. We performed a small

craniotomy over the area of interest (either PM or AL in distinct mice, identified using IOI) using a dental drill and inserted a glass pipette backfilled with AAV2.1-EF1a-double floxed-hChR2(H134R)-EYFP-WPRE-HGHpA (titer: 7×10^{12} vg/ml, 20 298-AAV1, Addgene). Four injections of 13.8 nL were made at two depths (two at 700 μm and two at 400 μm below the dura) using a Nanoject pressure injection system (Drummond Scientific Company). Each injection was spaced apart by at least 5 min from the next one to promote diffusion and prevent backflow. After viral injections, the recording chamber was covered with silicon elastomer (Picodent Twinsil) and mice were allowed to recover. In total, we performed successful injections in PM in 5 mice and in AL in 4 mice.

Craniotomy

After at least 3 weeks to allow for robust viral expression, mice were subcutaneously injected with the analgesic buprenorphine (0.025 mg/kg) and maintained under isoflurane anesthesia (induction at 3%, maintenance at 1.5–2%) during surgery. We performed small (200 μm) craniotomies over the areas of interest (V1 and either PM or AL) using a dental drill. The dura was left intact if possible. The recording chamber was sealed off with silicon elastomer and the mice were allowed to recover for 24 h.

In Vivo Electrophysiology

Mice were fixated in a custom-built holder in a dark and sound-attenuated cabinet. The body of the mouse was put in a tube (diameter: 4 cm) to limit body movements. The headbar was attached to a custom-made holder via two screws. Before recording sessions, mice were habituated to this type of head-fixation by daily progressive incremental time spent in head-fixation.

Recordings were performed either in an awake or anesthetized state and the order was counterbalanced across recording days. Under anesthesia, pure oxygen with isoflurane (at 0.6–1.2%) was delivered at 0.8 l/min. The level of anesthesia was monitored by observing breathing rate and neural activity. Isoflurane levels were slowly lowered over the course of a recording session to counteract tissue build-up and maintain a stable depth of anesthesia. Body temperature was monitored throughout and kept at 37.5 °C.

Extracellular recordings were performed with 32- or 64-channel microelectrode arrays (NeuroNexus—A1x32-Poly2-10 mm-50s-177, A4x8-5 mm-100-200-177, or A1x64-Poly2-6 mm-23 s-160). In each recording session, the electrode arrays were slowly inserted until the recording sites spanned the cortical layers. We verified visual responsiveness by displaying full-field gratings and reinserted the electrodes if there was no robust visual responsiveness in neural activity. The number of recording sessions was limited to 3 to minimize recording from a damaged circuit. For some recording sessions, electrodes were dipped in DiI (ThermoFisher Scientific) allowing better post-hoc visualization of the electrode

tract (Fig. 1C). After insertion, the exposed cortex and skull were covered with 1.3–1.5% agarose in artificial CSF to prevent drying and to help maintain mechanical stability. The ground was connected to the headbar and the reference electrode to the agarose solution. Recordings started at least 15 min after insertion to allow for tissue stabilization. Neurophysiological signals were amplified ($\times$1000), bandpass filtered (0.1–9 kHz), and acquired continuously at 32 kHz with a Digital Lynx 128 channel system (Neuralynx).

Optogenetics

To locally photostimulate PM or AL, a 473-nm laser (Eksma Optics, Vilnius, Lithuania, DPSS 473 nm H300) was connected with a fiber-optic patch cord to a fiber-optic cannula (ID 200 um, NA 0.48, DORIC lenses) that was positioned directly over the thinned skull at the area of interest. Photostimulation consisted of 10-ms pulses delivered at 20 Hz for the duration of visual stimulus presentation. Stimulus duration varied depending on the traversal time of the bar across the screen and, depending on traveled distance and speed of the bar, ranged from 0.45 s (vertical bar moving at 70 deg/s) to 6.3 s (diagonal bar moving at 20 deg/s). Light delivery was controlled by a shutter (Vincent Associates LS6 Uniblitz). During each session, we simultaneously performed extracellular recordings in the areas of interest (V1 and either PM or AL) and adjusted laser power to the minimum that maximally inhibited neural activity (range: 2–15 mW total power).

Visual Stimulation

Visual stimuli were gamma-corrected and presented with a 60-Hz refresh rate on an 18.5-inch monitor positioned at a 45° angle with the body axis from the mouse at 21 cm from the eyes, subtending 91° horizontally and 60° vertically. Three sets of visual stimuli were used.

Checkerboards: Before each session, we displayed full-field contrast-reversing checkerboards (full contrast, spatial frequency = 10 retinal degrees, temporal frequency of contrast reversal = 0.5 Hz, n = 10 reversals) to estimate laminar electrode positioning (see below).

Bars: Each bar stimulus consisted of a single white bar (luminance = 133 cd/m^2) drifting across an isoluminant gray screen (luminance = 32 cd/m^2) in one of eight directions at one of three speeds (20, 40s, or 70 deg/s) either in the absence or presence of photostimulation. Stimuli were separated by an intertrial interval of 3 s and repeated 20 times. The total trial set therefore consisted of 8 (orientations) × 3 (speeds) × 2 (photostimulation conditions) × 20 (repetitions) = 960 trials.

Gratings: Grating stimuli consisted of full-field drifting square-wave gratings (70% contrast) for 2 s, separated by 2 s intertrial interval. Similar to the bar stimuli, gratings drifted in one of eight directions at one of three speeds (20, 40, or 70 deg/s) either in the absence or presence of photostimulation for 20 repetitions. The
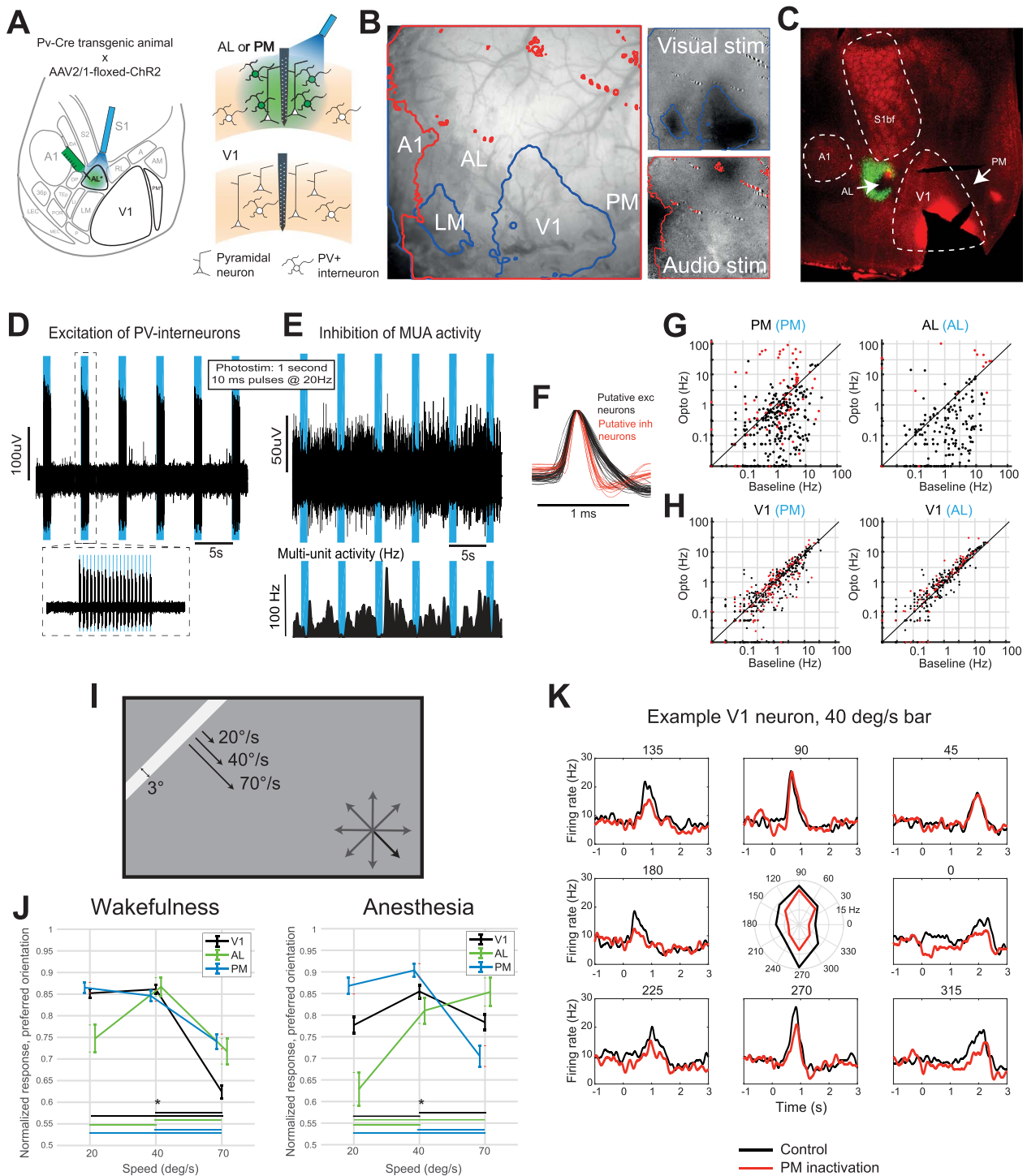
Fig. 1. Experimental setup. (A) Schematic of the experimental design. Left: top view of the left cortical hemisphere of a mouse, with subdivision in cortical areas—based on (Wang and Burkhalter 2007). Adeno-associated viral vector mediating the Cre-dependent expression of ChR2 was injected in area AL (or PM, not shown). During experiments, an optic fiber (blue) was placed on top of AL (or PM) to over-activate Cre-expressing PV+ interneurons and inactivate area AL (or PM). Right: scheme of coronal sections of either AL/PM (top) or V1 (bottom) showing laminar probe recordings in both areas. Expression of ChR2 and fiber-optic-mediated illumination were confined to area AL or PM (top). (B) Intrinsic signal imaging was used to localize cortical areas. Visual stimuli (top right) and auditory stimuli (bottom right) were used to activate and thus identify the location of visual and auditory cortices. The borders of visually and auditory-evoked signals (blue and red curves, respectively) were overlaid on the vessel map (left) to identify the location of V1, AL, and PM. In this example, V1, LM, and A1 were directly activated by visual or auditory stimuli. The location of AL and PM was determined based on published maps of the mouse visual system (see A). (C) Coronal section showing ChR2-conjugated GFP expression in area AL (green). Red reflects both the tdTomato fluorescent protein expressed in PV+ interneurons as well as the location of laminar probes stained with DiI. (D) Example neuronal trace from a PV+ interneuron recorded in area PM during optogenetic illumination in control trials (during awake recordings). Raw trace from a channel showing spiking activity evoked in a PV+ interneuron by optogenetic illumination. Blue areas indicate 1-s periods in which the blue laser was on. The inset shows the pattern of optogenetic illumination (10 ms ON—40 ms OFF) during each illumination period. (E) Top: Example multiunit activity (MUA) trace recorded in area PM during optogenetic illumination in control trials. In contrast with panel D, spiking activity decreased during illumination periods. Bottom: Firing rate traces as extracted from MUA activity shown above. Notice the decrease in firing rates during illumination. (F) Average action potential waveforms from a selection of putative excitatory neurons (black, characterized by broad spikes) and

Table 1. Number of recorded neurons

Bar speed	20 deg/s	40 deg/s	70 deg/s
PM inactivation—awake recordings	207	206	185
AL inactivation—awake recordings	94	97	79
PM inactivation—anesthetized recordings	88	87	87
AL inactivation—anesthetized recordings	67	65	63

three speeds were constructed based on combinations of spatial and temporal frequencies to optimize V1, PM, and AL responsiveness (Andermann et al. 2011; Marshel et al. 2011): Slow 20 deg/s: Spatial frequency = 0.1 cpd, Temporal frequency = 2 Hz, Mid 40 deg/s: Spatial frequency = 0.075 cpd, Temporal frequency = 3 Hz, Fast 70 deg/s: Spatial frequency = 0.057 cpd, Temporal frequency = 4 Hz.

Histology

At the end of the experiment, mice were overdosed with pentobarbital and perfused with 4% paraformaldehyde in phosphate-buffered saline, and their brains were recovered for histology. We cut coronal 50-μm sections with a vibratome, stained them with DAPI (0.3 μM), and imaged mounted sections to verify the viral expression and recording sites. The borders of individual higher visual areas in individual animals are not definable based on an atlas. However, with this consideration in mind, data from five animals were excluded based on weak expression in putative PM or AL or strong off-target expression beyond PM or AL or into V1.

Data Analysis
Spike Sorting

Before spike detection, the median of the raw trace of nearby channels (400 < um) was subtracted to remove artifacts. Spike detection and sorting were done using Klusta and manual curation using the Phy GUI (Rossant et al. 2016). During manual curation, each proposed

single unit was inspected based on its waveform, autocorrelation function, and firing pattern across channels and time. Only high-quality single units were included that 1) had an isolation distance higher than 10 (Schmitzer-Torbert et al. 2005), 2) had less than 0.1% of their spikes within the refractory period of 1.5 ms, and 3) were present throughout the session.

Classification of Neuron Subtypes

Putative pyramidal and putative fast-spiking interneurons were separated based on the peak-to-trough delay of their average normalized action potential waveform (Niell and Stryker 2008). The peak-to-trough delay was computed as the time between peak positive and peak negative voltage deflection (in ms), and single units with a delay lower than 0.45 ms were classified as narrow-spiking, while units with a delay higher than 0.55 ms were classified as broad-spiking. The rest remained unclassified. In total, 76.9% were labeled as broad spiking, 20.6% as narrow-spiking and 2.5% as unclassified.

Laminar Depth Estimation

The laminar depth of each electrode was estimated based on current source density analysis (CSD) of the local field potential (LFP) in response to contrast-reversing checkerboard stimuli (see above). The CSD profile was computed by applying standard Nicholson–Freeman calculations on the low-pass filtered signal (<100 Hz, fourth-order Butterworth filter) with Vaknin transform (Vaknin et al. 1988) with 0.4 Siemens per meter as conductivity. We

putative inhibitory neurons (red, characterized by narrow spikes). (G) Scatter plots of firing rates of individual neurons during spontaneous baseline activity and during optogenetic stimulation in areas PM (left) or AL (right, recording area in black font, photostimulated area in blue font between brackets), for both putative excitatory and inhibitory neurons (black and red points, respectively). Average spontaneous firing rates for putative excitatory neurons significantly decreased upon optogenetic stimulation of PM and AL in both areas (PM, $n = 338$ neurons, mean values: 2.3 and 1.0 Hz, $P = 1.31*10^{-26}$; AL, $n = 199$ neurons, mean values 2.5 and 0.9 Hz, $P = 2.06*10^{-21}$; Wilcoxon signed rank test), while those for putative inhibitory neurons increased significantly in AL ($n = 18$ neurons, mean values 8.6–24.3 Hz, $P = 0.0256$, Wilcoxon signed rank test), but not PM ($n = 72$ neurons, mean values: 3.4 and 13.1 Hz, $P = 0.08$, Wilcoxon signed-rank test). (H) Same as G, but for neurons recorded in V1 during optogenetic stimulation of either PM (left) or AL (right). Optogenetic stimulation of either PM or AL had minor but still significant effects on spontaneous activity in V1. Left: average spontaneous firing rates for V1 during optogenetic stimulation of PM significantly decreased for putative excitatory neurons: $n = 351$ neurons, 3.2 and 2.4 Hz, $P = 3.9*10^{-11}$, and putative inhibitory neurons: $n = 121$ neurons, 2.5–2.1 Hz, $P = 0.019$; Wilcoxon signed-rank test). Right: average spontaneous firing rates for V1 during optogenetic stimulation of AL significantly increased for putative excitatory neurons: $n = 283$ neurons, 2.8 and 2.9 Hz, $P = 0.041$, and putative inhibitory neurons: $n = 76$ neurons, 2.6–3.4 Hz, $P = 0.006$; Wilcoxon signed-rank test). Although spontaneous firing rates in V1 were affected by optogenetic stimulation in PM or AL, such increments or decrements were much weaker than those reported in PM and AL (see also Supplementary Fig. 1E). (I) Outline of the visual stimuli (moving bars moving at different speed along eight possible directions). (J) Speed preference for neurons located in V1 (black), PM (blue), and AL (green) as a function of brain state (left: wakefulness; right: anesthesia). For each neuron, responses to the preferred orientation were computed across the three bar speeds and normalized to the highest response (corresponding to the preferred bar speed). Asterisks indicate significant differences between speeds, for neurons located in the same area ($P < 0.05$, one-way Anova with post-hoc Tukey test; V1-awake: F = 109.41, $P = 3.13 \times 10^{-43}$; PM-awake: F = 18.5, $P = 1.8 \times 10^{-8}$; AL-awake: F = 8.19, $P = 0.0004$; V1-anesthetized: F = 5.79, $P = 0.0033$; PM-anesthetized: F = 27.47, $P = 1.8 \times 10^{-11}$; AL-anesthetized: F = 9.47, $P = 0.0001$). The number of neurons used for this analysis was: V1-awake: 339; V1-anesthetized: 158; PM-awake: 222; PM-anesthetized: 89; AL-awake: 70; and AL-anesthetized: 48. (K) PSTHs computed for an example neuron in V1, for bars moving at 40 deg/s across the eight different orientations, with and without optogenetic stimulation of area PM (black and red traces, respectively). The polar plot at the center of the panel shows the tuning curve of the example neuron.

calculated the CSD profile for each of the linear arrays of electrodes on our polytrode configuration separately and then merged the profiles. The electrode with the earliest visible sink was designated as the center of layer IV. Single units recorded from electrodes spanning 150 μm around this electrode were labeled as granular and units recorded from electrodes below and above this layer were labeled infra- and supragranular, respectively.

Firing Rate Response

To compute firing rates in response to visual stimuli, spikes times were aligned to stimulus onset, binned in 1-ms bins, and convolved with a Gaussian window (50-ms standard deviation). To compute single trial responses for bar stimuli, we first identified the time of peak response for each condition (orientation $\times$ speed) by averaging across trial repetitions without photostimulation. The response on each trial was obtained by averaging the single trial firing rate over 300 ms around this peak time ($\pm$150 ms), after subtracting baseline response (firing rates computed, separately for each trial, in the [−2000, −200] ms window before stimulus onset). In a set of control analyses, we averaged firing rates not over a fixed time window around peak time, but instead computed, as a function of bar speed, how much time a bar took to cover a certain portion of the visual field (5° or 10°, respectively). Time windows covering a receptive field of 5° corresponded to 500 ms at 20 deg/s, 250 ms at 40 deg/s, and 142 ms at 70 deg/s (and twice as much for a 10° coverage). For grating stimuli, the single-trial firing rate was averaged over 0–1000 ms after stimulus onset. Only neurons showing a significant sensory-evoked response (defined as having an average z-scored response > 1 for at least one bar direction) were retained for further analyses. Z-scoring was done by subtracting for each trial the mean firing rate of the baseline period (−1 to −0.2 s before stimulus) and dividing by the standard deviation of all baseline periods. Table 1 summarized the number of V1 neurons that were retained for analysis.

Quantification of Peak Latency, Tuning Curves, and Receptive Field Size

Peak response latency was defined as latency of the peak response (maximal z-scored firing rate) in the absence of optogenetic inactivation. This was determined for each direction and each speed separately and was determined only for those conditions in which a z-scored sensory-evoked response higher than 1 was found. Tuning curves for single neurons were quantified after computing, independently for each direction and separately for each speed, the firing rate response to a visual stimulus. The preferred orientation/direction was computed, separately for each speed, based on the bar direction eliciting the largest average firing rate response, in the absence of optogenetic inactivation. To align tuning curves, the preferred orientation of each neuron in the absence of optogenetic inactivation was

set to 0° and other orientations were displayed relative to this.

Receptive field size was computed separately for the average responses to each bar direction. We computed the response onset as the first time point after stimulus onset in which the z-scored firing rate response exceeded 1. The response offset was defined as the first time point following response onset for which the z-scored firing rate response dropped below 1. The receptive field size for a given direction was computed as the duration of the response (time lag between response onset and offset) multiplied by the speed of the bar. Receptive field size was aligned to the preferred direction, as described for the tuning curves.

Orientation and Direction Selectivity

Orientation and direction selectivity were computed using a global orientation selectivity index (gOSI) and a global direction selectivity index (gDSI) (Ringach et al. 2002; Mariño et al. 2005; Ibrahim et al. 2016). These two measures were computed as

$$gOSI = \frac{\left\| \sum_\theta R(\theta) e^{2i\theta} \right\|}{\sum_\theta R(\theta)}$$

and

$$gDSI = \frac{\left\| \sum_\theta R(\theta) e^{i\theta} \right\|}{\sum_\theta R(\theta)}.$$

Here, $R(\theta)$ is the baseline-corrected firing rate response of a neuron to a bar moving along direction θ and i is the imaginary unit. gOSI and gDSI vary between 0 and 1, with 0 indicating a neuron completely untuned for orientation/direction and 1 a neuron only responding to a single orientation/direction, respectively. For the analysis of gOSI and gDSI, we only retained neurons that showed significant sensory-evoked responses to at least one direction in the nonopto condition. If a neuron did not respond (meaning that no action potential was fired) to any stimulus direction in the opto condition, its gOSI and gDSI values were undetermined. For this reason, such neurons were removed from further analysis about how optogenetic inactivation affects gOSI and gDSI values.

Decoding Analysis

The population decoding analysis was done using a pseudo-population approach. Decoding was separately performed for awake and anesthetized recordings. All recorded neurons were pooled together (even if they were recorded in different sessions) and decoding was performed on a randomly selected number of neurons equal to the lowest available number of neurons per condition. For awake recordings, this amounted to 79 neurons; for anesthetized recordings, to 63 neurons (see the table above). In detail, we used the same number of neurons to decode the direction of a moving bar presented at every speed, without optogenetics or with

inactivation of either PM or AL; this procedure allowed us to fairly compare the different conditions (area being inactivated and bar speed). When pooling together data from different recording sessions, we only considered conditions (bars moving along a certain direction and speed) which had been repeated over at least 10 trials. For all conditions, 20 trials were sampled over recording sessions (with replacement, if fewer than 20 trials were present, and without replacement otherwise). These data were used to train a k-nearest neighbors classifier, which was trained to decode the direction of the bar being presented, based on the single-trial firing rate response (computed as described above as the average firing rate in a 300-ms window centered around the peak latency—here defined as latency of the peak response—of each neuron to a bar with a certain speed and direction). The performance of the decoder was assessed with a leave-one-out cross-validation procedure. Training was repeated 100 times, each time with a different, random set of neurons and randomly sampled trials. For each training set, we computed the average decoding error (difference between the presented direction of a moving bar and the estimated direction). Different decoding approaches (random forest, support vector machine) did not yield significantly better results. In a set of control analyses, we also computed decoding accuracy as the proportion of trials in which the direction of movement of a bar was correctly estimated.

Statistical Analysis

Statistical analyses were done using parametric methods (*t*-tests and ANOVAs) if the assumption of normality was not violated. This was verified via the use of a Kolmogorov–Smirnov test. Nonparametric tests were used otherwise. If applicable (i.e., when an Anova was performed), multiple comparisons were corrected using a Tukey post-hoc test. When multiple, independent comparisons were performed, *P*-values were corrected via the application of a Benjamini–Hockberg false discovery rate (FDR) procedure (Korthauer et al. 2019).

Data and Software Availability

Original data and the MATLAB, Python, and R scripts used to perform the analyses presented in this manuscript are available by reasonable request to Umberto Olcese (u. olcese@uva.nl).

Results

To investigate how HVAs influence V1 responses, we focused on two areas with the largest known differences in tuning to spatial and temporal frequencies of visual stimuli: AL and PM. While AL neurons preferentially respond to visual stimuli with high temporal frequencies and low spatial frequencies, the opposite is true for area PM (Andermann et al. 2011; Marshel et al. 2011). We performed dual-area silicon probe recordings in head fixed mice from either V1 and AL or V1 and PM

(Fig. 1A). Recordings were done in both the awake and anesthetized state. As recently reported (Keller et al. 2020), feedback modulation from HVAs to V1 is reduced under anesthesia, but the effect of brain state on V1 response properties is poorly understood (Olcese et al. 2018), although previous studies reported a reduction in direction tuning in isoflurane anesthesia compared with wakefulness (Goltstein et al. 2015). Localized nano-injections of a viral vector mediating Cre-dependent expression of channelrhodopsin were performed in either AL or PM of PV-Cre mice (Madisen et al. 2012)—Figure 1A,C. Areas V1, AL, and PM were localized via intrinsic optical signal imaging (IOI, Fig. 1B). We verified that expression was confined to AL or PM and did not extend across the PM-V1 or AL-V1 borders (Fig. 1C, Supplementary Fig. 1A–G). Blue-light illumination was used to inactivate either area AL or PM, via overactivation of parvalbumin-positive (PV+) interneurons (Olcese et al. 2013)—Figure 1D–G. We experimentally verified that optogenetic inactivation was confined to areas AL and PM and did not affect V1 directly (Fig. 1C,H). Specifically, inactivation of either AL or PM greatly reduced the activity of putative excitatory neurons in the illuminated area (Fig. 1G) but only had a minor effect of spontaneous firing activity in V1 (Fig. 1H) or non-photostimulated PM or AL (Supplementary Fig. 1H,I)—see also Supplementary Figure 1K. Furthermore, positioning the fiber tip over an uninfected control area (primary somatosensory area) did not affect firing rates in V1, excluding the possibility that scattered light reached the retina and affected visual responses (Supplementary Fig. 1J). The effectiveness of photostimulation in the target area increased as a function of laser power (Supplementary Fig. 1L). Moving bars were used as visual stimuli to evoke activity in V1 and HVAs (Fig. 1I). Compared with drifting gratings, moving bars enable to assess receptive field sizes of the recorded neurons (Niell and Stryker 2008). Bars were moving over eight different orientations at three different speeds, namely those that previous studies indicated as being preferred by PM (20 deg/s), V1 (40 deg/s), and AL (70 deg/s) (Andermann et al. 2011; Marshel et al. 2011). To verify this speed preference, we computed, separately for each neuron and area, the response to a bar moving along the preferred orientation, independently for each speed. For each neuron, responses were normalized to the speed evoking the strongest response (Fig. 1J). For recordings performed under anesthesia, the speed preference of neurons in each area was in line with the literature (Fig. 1J-right). During wakefulness, we found a shift for all areas to lower preferred speeds compared with anesthesia (Fig. 1J-left), although the differential speed preference of neurons in area PM and AL—with area PM selective for low speeds and AL for faster speeds—was preserved. Optogenetic inactivation of either area PM or AL strongly reduced sensory-evoked responses in putative excitatory neurons in the illuminated area—PM or AL, respectively (Supplementary Fig. 2). Inactivation of single HVAs also

reduced—to a lesser extent—sensory-evoked responses in V1 (Fig. 1K and Supplementary Fig. 3A,B, see also later sections). The reduction in V1 activity was, in contrast to the effect of the manipulation on PM and AL, limited to sensory-evoked responses, with only minor effects on spontaneous activity (Fig. 1G, Supplementary Fig. 1K) and can be interpreted in the first instance to be the consequence of impaired recurrent connectivity from AL or PM (see also Materials and Methods). We also tested whether temporally extended photostimulation during trials with low stimulus speeds might have an effect on V1 independent from optogenetics, but rather due to light-induced heating of the cortical tissue. Nevertheless, we found the effect of PM or AL inactivation on V1 to be independent of the duration of photostimulation (Supplementary Fig. 1M).

Inactivation of Areas AL and PM Globally Decreases V1 Responses to Moving Bars

Having established that areas AL and PM show sensory-evoked responses which differ based on the specific speed at which presented bars move (Fig. 1J), we wondered whether inactivation of AL and PM would differentially modulate V1 responses to bars moving at different speeds. Surprisingly, we found that inactivating either AL or PM consistently reduced V1 responses to bars moving at all the speeds we tested, and for both preferred and nonpreferred orientations (Fig. 2A–D, see also example traces of single neurons in Fig. 1K and Supplementary Fig. 3A,B). Importantly, direction preference was not modified by inactivation of PM and AL (Supplementary Fig. 4). This was the case during both awake (Fig. 2A–D) and anesthetized (Supplementary Fig. 5) recordings. We next asked if the extent to which V1 responses were reduced varied as a function of bar speed. For each neuron and bar speed, we computed the relative change in the response to a bar moving along the neuron's preferred direction following optogenetic inactivation of either area AL or PM. No significant difference was found between speeds when inactivating either AL or PM (Fig. 2E). Only for bars moving at 20 deg/s, we found than PM inactivation reduced V1 responses more strongly than AL inactivation. To further explore the possible occurrence of a functionally specific effect, we subdivided V1 neurons in three groups based on the bar speed for which they showed the highest response—cf. Huh et al. (2018)—and assessed whether AL and PM inactivation had different effects for the three groups of neurons. While we found no significant differences for bars (Fig. 2F), we did find some differences when presenting drifting gratings, in line with Huh et al. (2018)—see Supplementary Figure 6.

We also wondered if the reported effects of optogenetic inactivation of PM and AL on V1 responses could be at least partially ascribed to the characteristics of the measurements or to the methods we use to quantify sensory-evoked responses. To address this,

we first tested if the higher number of V1 neurons recorded during PM compared with AL inactivation might explain the different modulation of V1 responses that we observed for low speeds (Fig. 2E). We repeated the analysis of Figure 2E by resampling V1 neurons recorded during PM inactivation such that the same number of neurons was analyzed as was recorded during AL inactivation (see the legend of Supplementary Fig. 7A for details). While, as expected, the variability of response modulation following PM inactivation increased when the number of neurons used in the analysis decreased (Supplementary Fig. 7A), the main result reported in Figure 2E was preserved (Supplementary Fig. 7B, note the stronger reduction in responses following PM compared with AL inactivation only for bars moving at 20 deg/s). Furthermore, we tested if the results we obtained might depend on the temporal window used for quantifying sensory-evoked responses. Instead of a window of a fixed duration across speeds, we used a window of variable duration (still centered around peak responses), corresponding to the time a moving bar took to cover a visual angle of either 5° or 10°, irrespective of bar speed. In both cases, we confirm the results reported in Figure 2E (Supplementary Fig. 7C,D). Finally, we tested the use of geometric mean to compute across-neuron average modulation values. We observed similar results with respect to the use of arithmetic mean, but wider confidence intervals (cf., Fig. 2E, Supplementary Fig. 7E).

In conclusion, inactivating both AL and PM generally decreased V1 responses to moving bars. While we were able to confirm the previously reported presence of a functionally specific effect of AL and PM inactivation on V1 activity (i.e., being dependent on the speed preference of each HVA), this effect was weaker than the generalized decrease in responses observed across speeds (Fig. 2E,F, Supplementary Fig. 6).

Inactivation of AL and PM Decreases Responses to Stimuli Entering the Receptive Field of V1 Neurons

The general reduction in visually evoked responses (Figs 1K and 2A,C) made us wonder whether inactivating areas PM and AL would also reduce the receptive field size of V1 neurons. Since we used moving bars, any estimate of receptive field size computed through responses to such stimuli is conflated with response amplitude (unlike estimates made via the use of nonmoving stimuli). Therefore, in line with the reduction in amplitude and duration of responses to moving bars (Fig. 2) in awake recordings, we also observed a reduction of receptive field size, which was especially pronounced for bars moving at low speed (20 deg/s; Fig. 3A,D) but still present for bars moving at higher speeds, albeit only for some orientations (Fig. 3A,D). Nevertheless, the use of moving bars also allowed us to assess whether receptive field size (which, as we mentioned, goes in parallel with the size of sensory-evoked responses) is differentially affected by inactivation of PM and AL based on whether
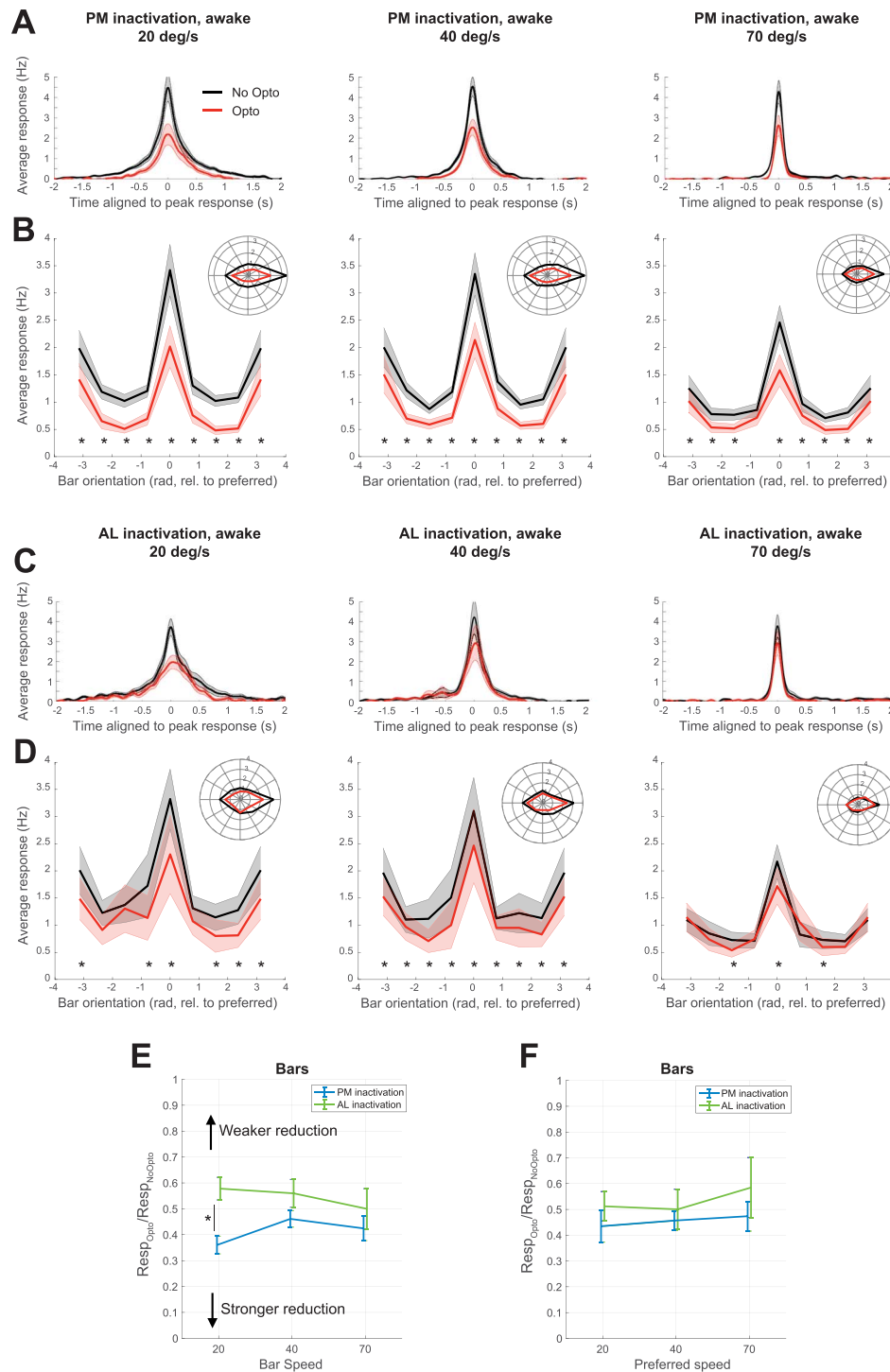
Fig. 2. Optogenetic inactivation of area AL and PM during wakefulness depresses sensory-evoked responses in V1. (*A*) PSTHs (aligned to peak latency in the absence of optogenetic inactivation) averaged over all V1 neurons responding to visual stimuli during awake recordings in the absence or presence of optogenetic inactivation of area PM (black and red curves, respectively). Curves with shading indicate mean ± SEM. From left to right: responses to bars moving at 20, 40, and 70 deg/s. (*B*) Tuning curves of average responses of V1 neurons during awake recordings to bars moving at different orientation (aligned by the preferred orientation in the absence of optogenetic inactivation, which is set at 0 rad) in the absence or presence of optogenetic inactivation of area PM (black and red curves, respectively). Curves with shading indicate mean ± SEM. Inset: Average response displayed in polar coordinates. Asterisks indicate significant differences between responses to bars moving at a given orientation in the absence or presence of PM inactivation ($P < 0.05$, paired *t*-test, FDR-corrected). From left to right: responses to bars moving at 20, 40, and 70 deg/s. (*C*) Same as *A*, but now for the inactivation of area AL. (*D*) Same as *B*, but now for the inactivation of area AL. (*E*) Relative effect of optogenetic inactivation of either PM (blue) or AL (green) on V1 responses evoked by moving bars during awake recordings ($\text{Resp}_{\text{Opto}}/\text{Resp}_{\text{NoOpto}}$), as a function of bar speed. Asterisks indicate significant differences either between speeds (for a given area) or between inactivation of distinct areas, given the same speed ($P = 0.0009$, two-way Anova with post-hoc Tukey test: significant main effect for inactivated area [$F = 4.83$, $P = 0.028$]). Error bars indicate mean ± SEM. (*F*) Same as *E*, but subdividing neurons based on their preferred speed, and only considering the effect of optogenetic inactivation on the preferred speed. The number of neurons included in the analyses shown in the figure is provided in Table 1.

a stimulus is entering or leaving the receptive field of a neuron. This is an important question in view of the possible role of HVAs in predictive processing (Keller et al. 2020). To address this, we separately computed the receptive field size in the rising phase of the evoked response (from response onset to peak response) compared with the decaying phase (after peak response)—see the inset in Figure 3B. We performed this analysis for responses to stimuli moving along each neuron's preferred direction. After inactivation of either area PM or AL, responses during the rising phase became more spatially localized, that is, neurons start responding later to moving bars entering the receptive field compared with control conditions (Fig. 3B,D). Receptive field sizes during the decay phase (i.e., for bars leaving the receptive field) were generally unchanged, except for an increase for bars moving at 40 deg/s upon PM inactivation (Fig. 3B,D). The preferential effect of HVA inactivation on the rising phase of the response to the preferred orientation can also be observed in the single neuron examples in Figure 1K and Supplementary Figure 3A. Results were very similar for recordings performed under anesthesia, with the main difference being larger receptive fields for V1 neurons in anesthetized than in awake recordings (Supplementary Fig. 8). Thus, inactivating AL and PM specifically reduces and delays V1 responses to moving bars entering the receptive field of V1 neurons, in line with a role of HVAs in generating predictions about upcoming visual stimuli.

Orientation and Direction Selectivity of V1 Neurons Are Enhanced for Moving Bars when AL and PM Are Inactivated

To better explore the functional significance of the reduction in V1 responses and receptive field size, we wondered how inactivating AL and PM might affect orientation and direction selectivity of V1 neurons. These were quantified by computing, respectively, a gOSI and a gDSI (Ringach et al. 2002; Mariño et al. 2005; Ibrahim et al. 2016)—see Materials and Methods. Values of gOSI and gDSI were in line with those previously reported for mouse V1 (Ibrahim et al. 2016). Based on previous literature (Pafundo et al. 2016), we hypothesized that inactivation of HVAs would reduce both gOSI and gDSI. To our surprise, both gOSI and gDSI instead increased, across all bar speeds and in both wakefulness and anesthesia, regardless of whether AL or PM was inactivated (Fig. 4A–D, Supplementary Fig. 9). No significant difference was found between inactivation of AL or PM, or between bar speeds (Fig. 4E,F)—although a more prominent enhancement for both gOSI and gDSI was observed at low speeds compared with high speeds when PM was inactivated during anesthesia (Supplementary Fig. 9). The increase in orientation and direction selectivity was observable in single neurons (Fig. 1K, Supplementary Fig. 3A,B) and in peak-normalized tuning curves (Supplementary Fig. 3C,D). Overall, these results suggest that, in contrast with

previous literature (Pafundo et al. 2016), inactivation of AL and PM differentially reduces responses to bars moving along preferred and nonpreferred orientations, in a way that enhances orientation and direction selectivity.

Single-Trial Decoding of the Orientation of Moving Bars Improves in V1 during Wakefulness Following Inactivation of AL or PM

Orientation and direction selectivity indices are computed over average responses to visual stimuli. Therefore, we wondered if, in spite of enhancing gOSI and gDSI, inactivating AL and PM might have a different effect at the single-trial level. We reasoned that a reduction in the amplitude of sensory-evoked responses might also reduce response variability at the average level. Thus, the improved gOSI and gDSI that we reported could be the consequence of both a reduction in response variability as well as of differential changes in sensory-evoked responses to stimuli moving along preferred versus nonpreferred orientations. On the other hand, single-trial response selectivity would directly reflect changes in sensory-evoked responses and not a reduction in across-trial variability. Thus, we implemented a pseudopopulation-based decoding approach (i.e., performed by pooling together neurons recorded in different sessions and animals) to measure how well the direction of moving bars could be decoded from single-trial V1 responses (see Materials and Methods). In line with the increase in gOSI and gDSI, we found that, during awake recordings, inactivating AL or PM significantly enhanced single-trial decoding of bar orientation, irrespective of bar speed, and with a stronger improvement following AL than PM inactivation (Fig. 5). Notably, decoding error in control conditions was relatively high (~70°), but decoding performance was comparable to recent literature (Cai et al. 2018) when quantified as the percentage of correctly classified directions (Supplementary Fig. 10A). Importantly, decoding performance vastly improved upon inactivation of PM or AL (40°). Similar results were observed for recordings under anesthesia, although the improvement in decoding following inactivation of PM or AL was smaller than for awake recordings (Supplementary Fig. 10B). Thus, inactivation of AL and PM not only reduces visually evoked responses and makes receptive fields smaller (i.e., spatially more precise) but also—possibly by differentially affecting responses to bars moving along preferred versus nonpreferred orientations and directions—enhances the selectivity of V1 neurons to the orientation and direction of moving stimuli, both at the average and single-trial level.

AL and PM Provide a Modulatory Gain to V1, which Enhances Weak Visual Responses during Wakefulness

The above results paint a counter-intuitive role of AL and PM, which would have a primarily detrimental role on the response selectivity of V1 neurons if their sole
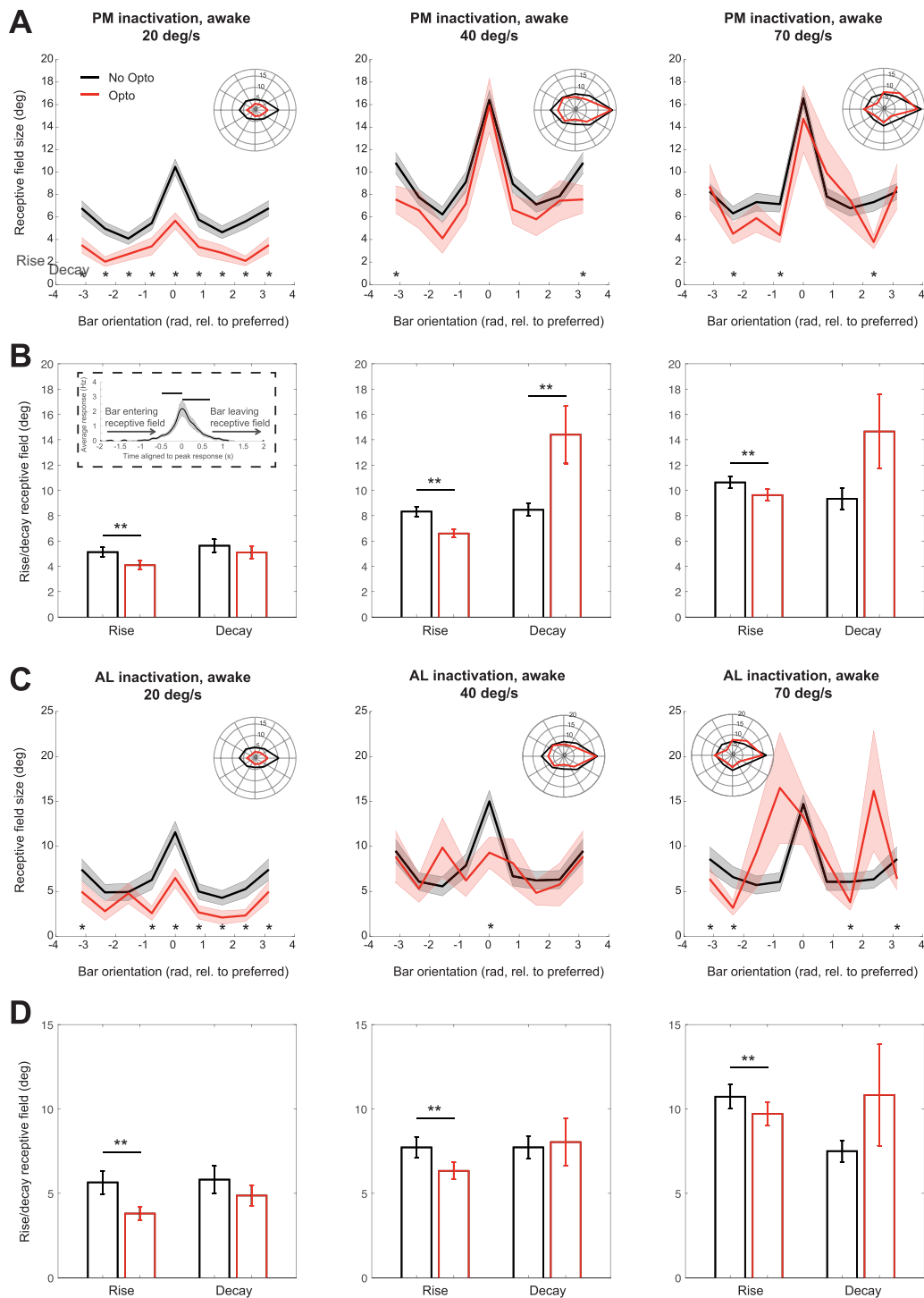
Fig. 3. Optogenetic inactivation of area AL and PM during wakefulness asymmetrically reduces receptive field size of V1 neurons in the rising but not in the decaying phase of sensory evoked responses. (A) Tuning curves of receptive field size of V1 neurons during awake recordings to bars moving at variable orientation (aligned by the preferred orientation, which is set at 0 rad) in the absence or presence of optogenetic inactivation of area PM (black and red curves, respectively). Curves with shading indicate mean ± SEM. Inset: average receptive field size displayed in polar coordinates; preferred orientation is aligned to the 0 deg (rightward) direction. Asterisks indicate significant differences between receptive field size to bars moving at a given orientation in the absence or presence of optogenetic inactivation of area PM ($P < 0.05$, paired *t*-test, FDR-corrected). From left to right: responses to bars moving at 20, 40, and 70 deg/s. (B) Receptive field size computed in the rising or decaying phase of sensory-evoked responses to moving bars moving along the direction preferred by individual neurons (from stimulus onset to peak response and after peak response, respectively) in the absence or presence of optogenetic inactivation of area PM (black and red bars, respectively). Bars indicate mean ± SEM. Asterisks indicate significant differences between receptive field sizes measured in the absence or presence of optogenetic inactivation of area PM (paired *t*-test; $*P < 0.05$, $**P < 0.01$). From left to right: responses to bars moving at 20, 40, and 70 deg/s. (P-values for significant differences: 20 deg/s rising phase $P = 1.2 \times 10^{-6}$; 40 deg/s rising phase $P = 6.8 \times 10^{-10}$; 70 deg/s rising phase $P = 3.1 \times 10^{-6}$; 40 deg/s decay phase $P = 0.008$). The inset shows an example PSTH (same as Fig. 2A) to graphically explain what the rising and decaying phases correspond to. (C) Same as A, but now for optogenetic inactivation of area AL. (D) Same as A, but now for optogenetic inactivation of area AL. (P-values for significant differences: 20 deg/s rising phase $P = 0.0003$; 40 deg/s rising phase $P = 0.0007$; 70 deg/s rising phase $P = 0.0037$). The number of neurons included in the analyses shown in the figure is provided in Table 1.
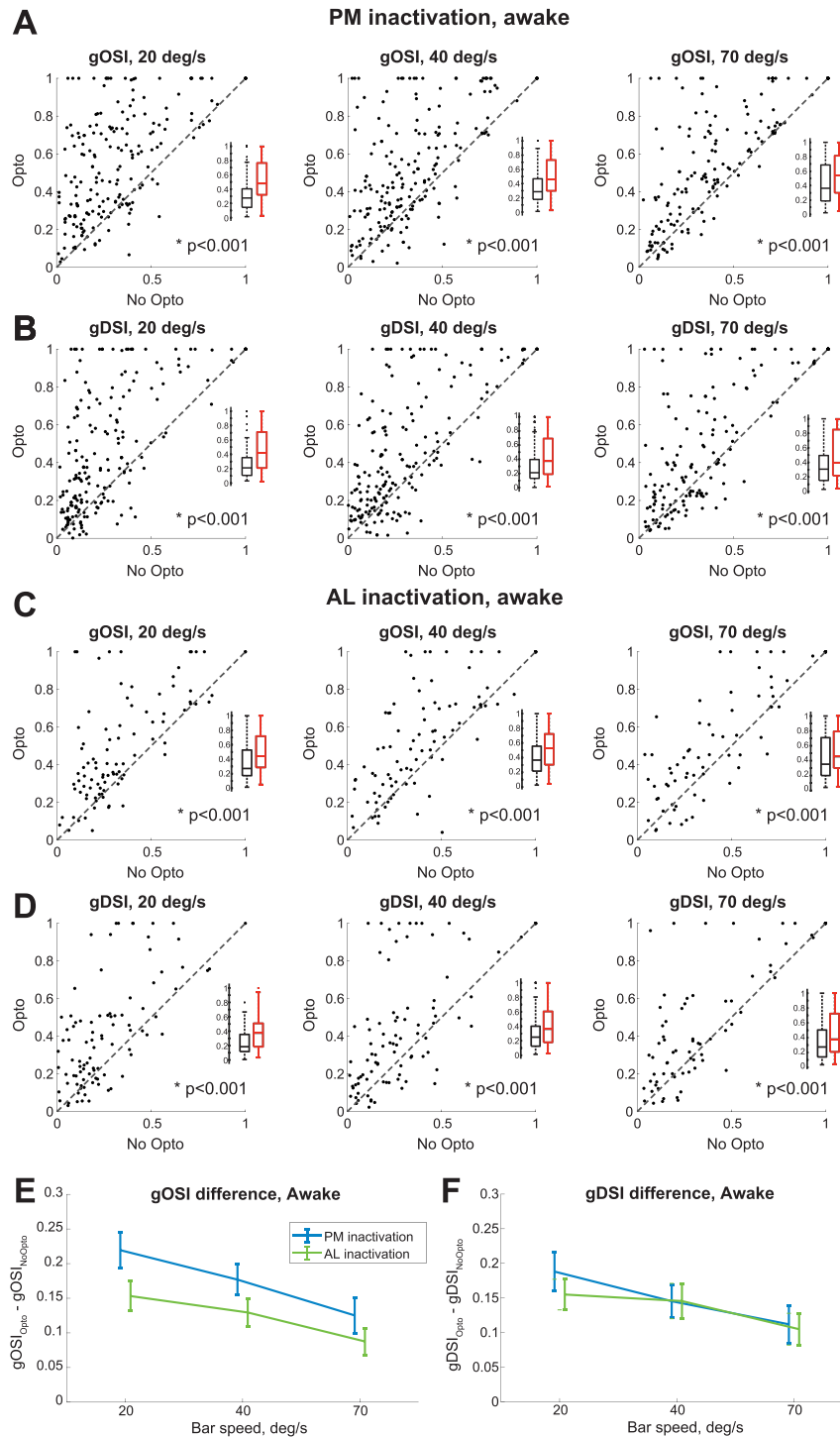
Fig. 4. Optogenetic inactivation of area AL and PM during wakefulness enhances orientation and direction selectivity in V1. (A) Scatter plots showing the orientation selectivity of V1 neurons during awake recordings in the absence or presence of optogenetic inactivation of area PM (x and y axis, respectively). Each point corresponds to a single neuron. Asterisks indicate significant differences between gOSI for bars moving at a given orientation in the absence or presence of optogenetic inactivation of area PM (see exact P-value in each panel, Wilcoxon signed rank test). From left to right: gOSI for bars moving at 20, 40, and 70 deg/s. In each panel, boxplots depict descriptive statistics for gOSI values in No-Opto and Opto conditions (black and red, respectively). (B) Same as A, but now for direction selectivity (gDSI). (C) Same as A, but now for optogenetic inactivation of area AL. (D) Same as B, but now for optogenetic inactivation of area AL. (E) Average change in the orientation selectivity of V1 neurons during awake recordings as a function of bar speed and area being inactivated (PM: blue; AL: green). Error bars indicate mean ± SEM. No significant difference was found, neither between bar speeds nor between areas. (F) Same as E, but now for direction selectivity. No significant difference was found, neither between bar speeds nor between areas. The number of neurons included in the analyses shown in the figure is provided in Table 1.
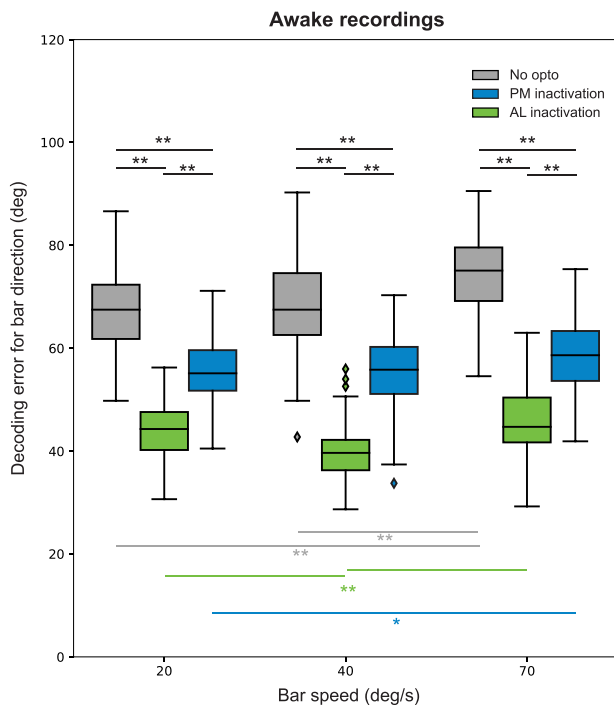
Fig. 5. Optogenetic inactivation of area AL and PM during wakefulness enhances single-trial decoding of bar orientation in V1. Boxplots show the error (in deg) made by a decoder trained to estimate the orientation of a moving bar presented during individual trials, from the activity of a pseudo-population of V1 neurons (see Materials and Methods for decoding analysis). A lower decoding error indicates better ability to decode the orientation of a moving bar. Boxplots were separately computed for trials without optogenetic stimulation (gray) and for trials in which either AL (green) or PM (blue) was inactivated. Asterisks indicate significant differences (∗$P < 0.05$, ∗∗$P < 0.001$; two-way Anova with post-hoc Tukey test (main effect for inactivated area: $F = 1056.6$, $P = 0.0000$; main effect for bar speed: $F = 56.6$, $P = 0.0000$; interaction effect: $F = 3.7$, $P = 0.0052$). The number of neurons included in the analyses shown in the figure is provided in Table 1.

purpose was to signal the orientation and direction of visual stimuli. We thus investigated in more depth whether inactivating AL and PM has a differential effect based on the size of a neuron's response to a given orientation. We reasoned that the modulation provided by AL and PM onto V1 might differentially enhance responses of different sizes (such as those elicited by bars moving along preferred vs. nonpreferred orientations and directions), as previously shown for other forms of cortical gain modulation (Ferguson and Cardin 2020). If the role of AL and PM is to selectively enhance small V1 responses, to enhance the reliability of responses to— for instance—small sensory stimuli just entering the receptive field of a neuron, this might also explain the depressed orientation and direction selectivity which PM and AL induce. To test this, we first assessed whether AL and PM might provide a form of additive or multiplicative gain modulation of V1 responses, as these are often found in visual cortex (Wilson et al. 2012). To this aim, we subtracted or divided V1 responses following optogenetic inactivation of AL and PM by V1 responses in control conditions (Fig. 6A,B). During awake recordings, AL and PM implemented neither an additive nor a multiplicative form of gain modulation.

In case of additive modulation, the curves in Figure 6A would have been flat, reflecting a similar reduction in evoked responses following inactivation of AL or PM; similarly, in case of multiplicative modulation, the curves in Figure 6B would not have shown differences between preferred and nonpreferred bar directions. Conversely, inactivating AL and PM reduced the responses of V1 neurons to their preferred orientation significantly more than (weaker) responses to nonpreferred orientations in terms of absolute difference (Fig. 6A), thus indicating a nonadditive form of modulation. Similarly, in terms of relative amplification (division between responses with or without optogenetic inactivation of AL or PM), responses to preferred orientations were reduced less than smaller responses to nonpreferred orientations (Fig. 6B). Next, we computed how optogenetically induced response difference ($Resp_{NoOpto}$-$Resp_{Opto}$) and response amplification ($Resp_{Opto}$/$Resp_{NoOpto}$) of V1 sensory-evoked responses vary as a function of the amplitude of sensory-evoked responses (irrespective of the orientation/direction of the moving bar to which a response is made). For the inactivation of both PM and AL, V1 responses were modulated in a way that does not conform to either an additive or multiplicative model (cf., the colored and gray lines in Fig. 6C,D). Low-amplitude responses were more strongly suppressed than high-amplitude ones, with a cutoff present at ~3 Hz (Fig. 6C,D), which is in line with our earlier analyses about the modulation of responses to preferred versus nonpreferred directions. The nonuniformity of response modulation was significant in all instances ($P < 2 \times 10^{-16}$, Chi-square goodness of fit test against a uniform distribution) and similar results were found under anesthesia (Supplementary Fig. 11). Altogether, these results show that AL and PM provide a form of gain modulation that selectively enhances weak responses of V1 neurons, such as those evoked by bars moving along nonpreferred orientations and directions. To investigate whether this amplitude-dependent modulation applies to all V1 neurons, independently from their response amplitude and orientation selectivity, we stratified V1 neurons based on either the amplitude of the sensory-evoked responses or the value of gOSI. Irrespective of whether we focused on the top or bottom 50% for the responses to the preferred orientation or the gOSI, we found that optogenetic inactivation of PM and AL invariably decreased responses to both preferred and nonpreferred orientations (although the latter were more strongly impacted) and enhanced gOSI (Supplementary Fig. 12A–D). This suggests that PM and AL do not implement a selective suppression of weakly responsive or nonselective neurons, or specifically reduce (or even suppress) low-amplitude responses. Rather, inactivation of PM and AL similarly affects all V1 neurons and sensory-evoked responses, albeit in a way that nonlinearly depends on response amplitude (Fig. 6C,D). Furthermore, we asked if the enhanced orientation and direction selectivity that we reported
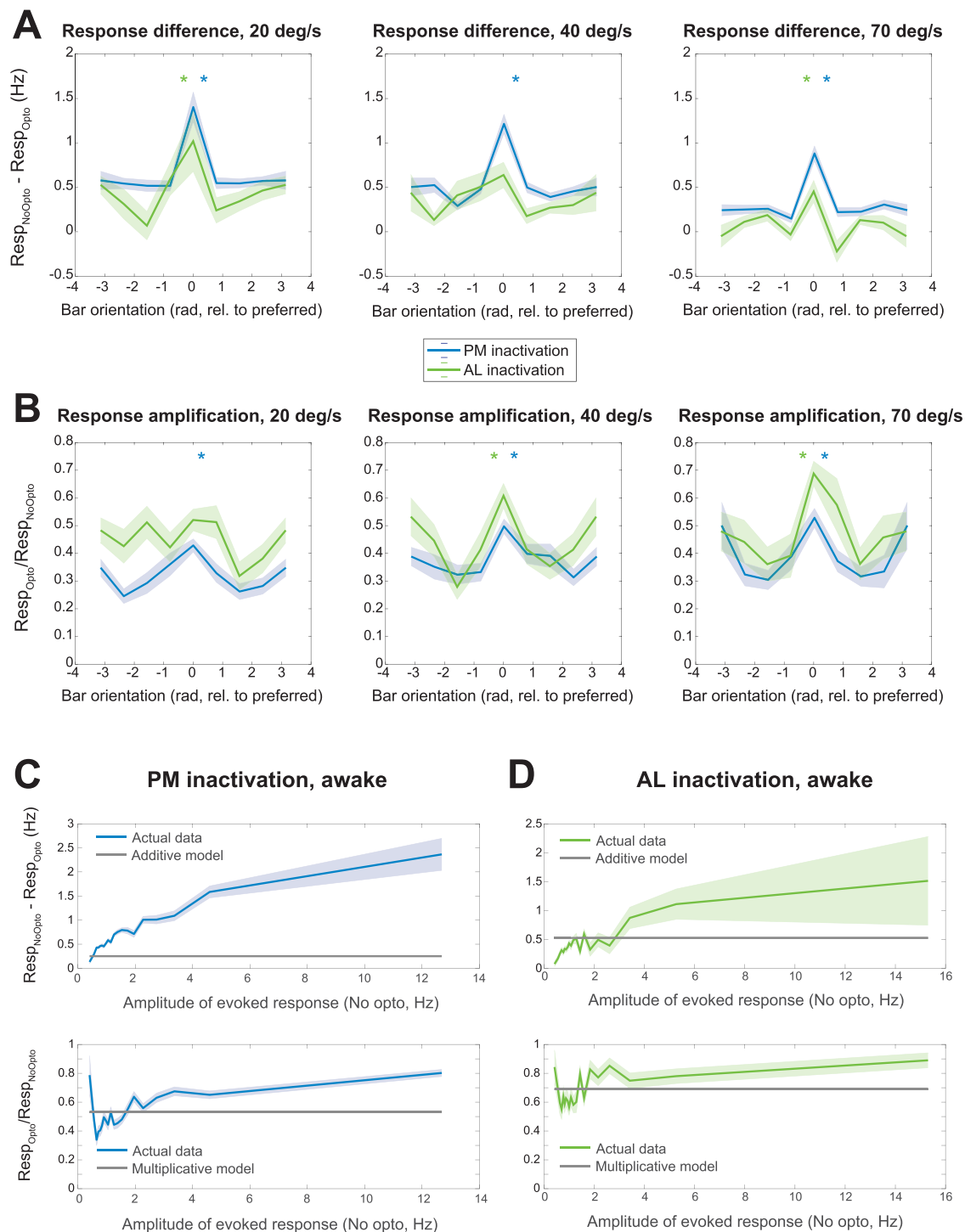
Fig. 6. Areas AL and PM enhance visual responses in V1 during wakefulness neither by additive nor multiplicative gain. (A) Difference in sensory-evoked responses of V1 neurons in the absence or presence of optogenetic inactivation of either area PM (blue lines) or AL (green lines) during awake recordings, separately for each orientation of a moving bar—respectively—at 20 deg/s (left), 40 deg/s (middle), or 70 deg/s (right). Curves with shading indicate mean ± SEM. The asterisks indicate if, separately for each bar speed and area (as indicated by color of asterisk), the difference in sensory-evoked responses was the same for all orientations (null hypothesis, corresponding to a flat line in the plot), or not ($P < 0.05$, one way Anova; a post-hoc Tukey test revealed a larger difference for the preferred orientation corresponding to 0 rad; for PM—20 deg/s: $F = 12.43$, $P = 1.4 \times 10^{-15}$; for PM—40 deg/s: $F = 15.02$, $P = 4.0 \times 10^{-19}$; for PM—70 deg/s: $F = 17.12$, $P = 7.0 \times 10^{-22}$; for AL—20 deg/s: $F = 2.54$, $P = 0.0136$; for AL—40 deg/s: $F = 1.68$, $P = 0.1102$; for AL—70 deg/s: $F = 4.66$, $P = 4.2 \times 10^{-5}$). (B) Same as A, but now for the ratio between sensory-evoked responses of V1 neurons in the presence or absence of optogenetic inactivation of either area PM (blue lines) or area AL (green lines). In general, responses to the preferred orientation were reduced less by optogenetic inactivation of area PM or AL, compared with responses to nonpreferred orientations ($P < 0.05$, one-way Anova with post-hoc Tukey test; for PM—20 deg/s: $F = 3.59$, $P = 0.0008$; for PM—40 deg/s: $F = 2.87$, $P = 0.0056$; for PM—70 deg/s: $F = 3.01$, $P = 0.0038$; for AL—20 deg/s: $F = 1.91$, $P = 0.0645$; for AL—40 deg/s: $F = 3.39$, $P = 0.0014$; for AL—70 deg/s: $F = 2.46$, $P = 0.0168$). (C) Curves showing difference and amplification (top and bottom panel, respectively) of V1 responses following PM inactivation as a function of the amplitude of sensory-evoked responses under unperturbed conditions. Sensory-evoked responses (*x*-axis) were divided into 20 equipopulated bins and, for each bin, the mean ± SEM value of optogenetic-induced responses difference or amplification was computed (solid blue line and shading, respectively). The gray line indicated the response difference or amplification obtained when applying an additive (top panel) or a multiplicative (bottom panel) model—see Materials and Methods for details.

following inactivation of PM and AL might be amplified or even caused by the occurrence of few, spurious spikes occurring in neurons which would have otherwise been silenced. To answer this question, we focused on the subset of neurons showing gDSI = 1 in the opto condition. These neurons maintained their direction preference (albeit with lower direction and orientation selectivity) in the no-opto condition (Supplementary Fig. 12E), which indicated that even these extreme values of gDSI are not an artefactual consequence of optogenetic inactivation.

To further explore the mechanism underlying this form of gain modulation, and in particular whether AL and PM targeted specific neuronal subpopulations in V1, we subdivided neurons based on whether their action potential waveform was broad or narrow, that is, corresponding to a putative pyramidal or fast-spiking interneuron, respectively (Olcese et al. 2013, 2016; Vinck et al. 2015), and based on whether neurons were located in supragranular, granular, or infragranular layers (see Fig. 7A–C and Materials and Methods). However, no difference was observed between putative excitatory and inhibitory neurons nor between putative excitatory neurons residing in different cortical layers as concerns changes in visual responses following inactivation of AL and PM (Fig. 7D–G). Therefore, the modulation provided by AL and PM onto V1 seems to similarly affect all major neuronal components of V1.

Discussion
Areas AL and PM Impact Mostly on Weak Sensory-Evoked Responses in V1

Inactivation of either area AL or PM similarly reduced sensory-evoked responses in V1 (Fig. 2). Therefore, the main role of AL and PM, in our paradigm, is to enhance sensory-evoked responses in V1, in particular weaker ones such as those to nonpreferred stimuli (Fig. 6) and those occurring in the early phase of sensory-evoked responses (Fig. 3). It was previously shown that inactivating HVAs (Pafundo et al. 2016) or feedback projections from HVAs onto V1 (Huh et al. 2018) decrease sensory-evoked responses in V1. However, in previous studies, the effects were either limited to responses to the preferred orientation (Pafundo et al. 2016), were specific for the receptive field center and not the surround (Nurminen et al. 2018), or were functionally specific (i.e., related to the tuning properties of individual HVAs). For instance, Huh et al. (2018) reported that inactivation of feedback projections from AL or PM onto V1 specifically reduced responsiveness of V1 neurons tuned to spatial frequencies similar to those of AL or PM. In contrast, we observed

a generalized decrease in V1 responses and receptive field size that was independent of the speed tuning of either AL, PM, or individual V1 neurons. This functionally aspecific effect (at least for what pertains speed tuning for moving bars) is even more unexpected when considering that anatomical projections from HVAs onto V1 are also functionally specific (Marques et al. 2018) and target patches in layer 1 of V1 (Ji et al. 2015; D'Souza et al. 2019) based on factors such as orientation/direction tuning and speed preference. How are these two apparently discordant effects compatible?

First, most previous studies focused on the lateromedial (LM) secondary visual area (Pafundo et al. 2016; Marques et al. 2018). LM is thought to be part of the mouse ventral stream, while both AL and PM are attributed to the dorsal stream (Wang et al. 2012). Thus, the roles of area LM versus AL and PM in modulating activity in V1 might be different, also in view of the specific functions of LM in higher order visual processing (Khastkhodaei et al. 2016; Tafazoli et al. 2017; Matteucci et al. 2019; Pak et al. 2020). Inactivation of LM primarily affects the superficial layers of V1 (Pafundo et al. 2016); conversely, in our study, inactivation of AL or PM similarly affected all the major subpopulations of V1. Furthermore, none of the prior studies used moving bars, but drifting gratings. Gratings are commonly displayed over a larger field of view compared with bars (which, in our case, were only 3° wide stimuli). Thus, moving gratings simultaneously evoke activity in a larger population of neurons compared with bars. Therefore, at the population level, moving bars elicit an overall instantaneous weaker activity compared with gratings. The aspecific modulatory effect we report primarily affects weak responses to visual stimuli, but it is possible that it might occur jointly with a functionally specific form of modulation (i.e., dependent on the spatial and temporal tuning properties of HVAs and V1 neurons), such as that described for instance in Huh et al. (2018). Indeed, when we performed preliminary experiments with drifting gratings, we found results in line with Huh et al. (2018). Nevertheless, it is striking that we did not observe any functionally specific effect with bars moving at different speeds, given that speed tuning of AL and PM are among the most different among HVAs (Andermann et al. 2011; Marshel et al. 2011). Another difference between our study and Huh et al. (2018) is that we completely inactivated AL and PM, and not just the neurons in these areas projecting back to V1. It may be the case that inactivation of a network node, and not just of feedback-projecting neurons, may have a broader, less specific effect, which may be due to a combination of

---

Optogenetic inactivation of area PM modulates sensory-evoked V1 responses in a way that is different from both an additive or multiplicative model. In particular, the bottom plot shows how optogenetic inactivation of area PM more strongly suppressed low-amplitude compared with high-amplitude sensory-evoked responses ($P < 2 \times 10^{-16}$, Chi-square goodness of fit test against a uniform distribution). (D) Same as E, but now for the inactivation of area AL. As for inactivation of PM, inactivation of AL modulates sensory-evoked V1 responses in a way that is different from both an additive or multiplicative model. Also, low-amplitude sensory-evoked responses are more strongly suppressed compared with high-amplitude sensory-evoked responses ($P < 2 \times 10^{-16}$, Chi-square goodness of fit test against a uniform distribution). The number of neurons included in the analyses shown in the figure is provided in Table 1.
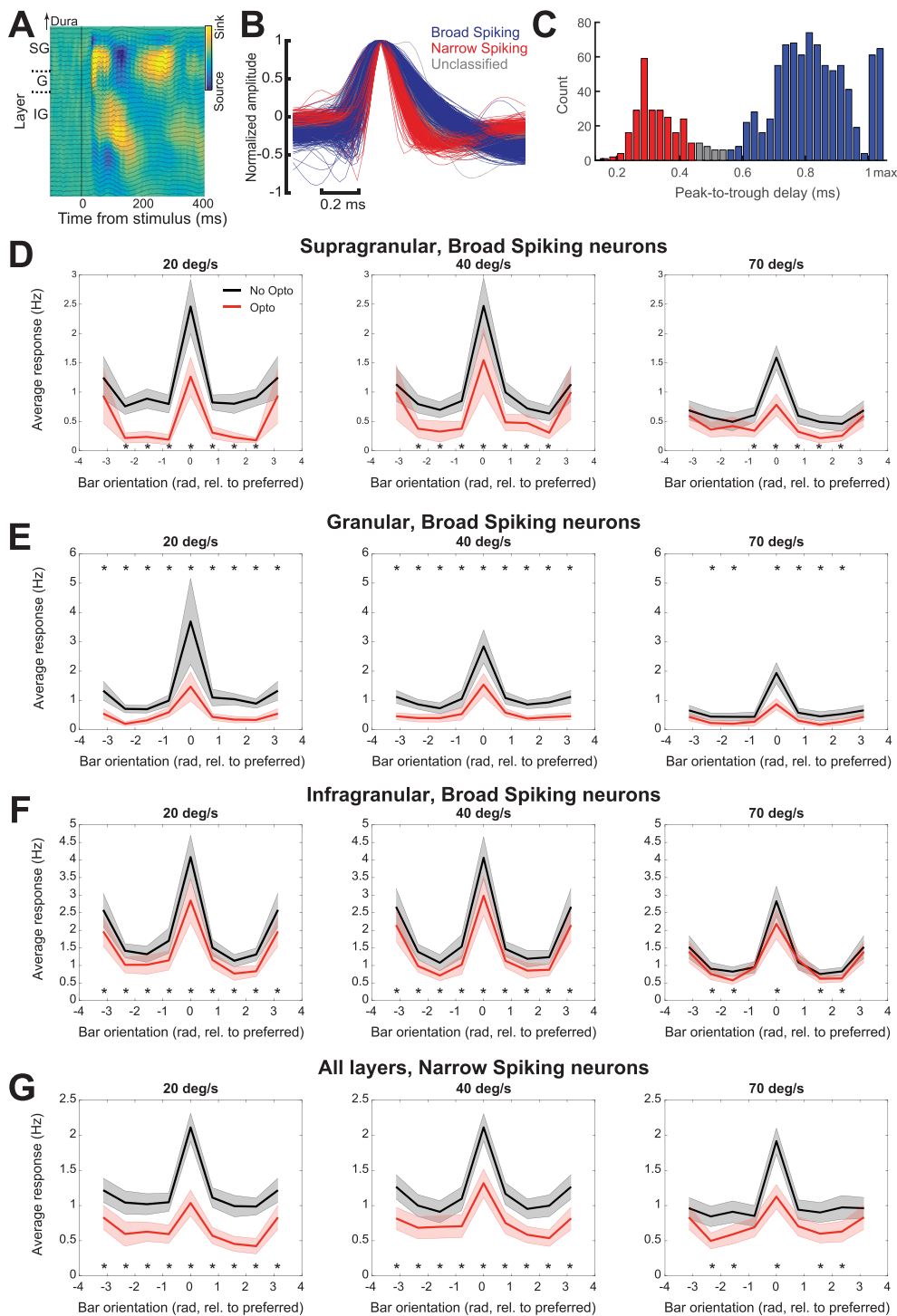
Fig. 7. Optogenetic inactivation of area AL and PM during wakefulness similarly affects distinct V1 neuronal subpopulations. (A) CSD profile of average response to checkerboard stimulation across layers of V1. The bottom of the earliest sink after checkerboard onset was used to demarcate the boundary between L4 and L5—as in (Schnabel et al. 2018). We used this in combination with registered depth of penetration of the silicon probe relative to the cortical surface, to align electrode depth across recordings sessions. Black traces show the LFP traces of each channel along the electrode tract. (B) Normalized waveforms for each individually recorded V1 neuron, averaged over all recorded action potentials, and colored by their classification based on peak-to-trough delay (blue: broad spiking neuron; red: narrow spiking neuron; gray: undetermined). (C) Histogram of peak-to-trough delay for the three classes. Bars at maximum indicate neurons whose trough extended beyond the sampled time around the action potential (2 ms). (D) Tuning curves of average responses of broad spiking V1 neurons located in supragranular layers of V1 during awake recordings to bars moving at different orientation (aligned by the preferred orientation, which is set at 0 deg) in the absence or presence of optogenetic inactivation (black and red curves, respectively). Recordings performed during the inactivation of PM and AL were pooled together. Curves with shading indicate mean ± SEM. Asterisks indicate significant differences between responses to bars moving at a given orientation in the absence or presence of optogenetic inactivation ($P < 0.05$, paired t-test, FDR-corrected). From left to right: responses to bars moving at 20, 40, and 70 deg/s. The number of neurons included in this analysis was 34 (20 deg/s), 34 (40 deg/s), and 29 (70 deg/s). (E) Same as D, but now for broad spiking V1 neurons in granular layers. The number of neurons included in this analysis was 28 (20 deg/s), 30 (40 deg/s), and 28 (70 deg/s). (F) Same as D, but now for broad spiking V1 neurons in infragranular layers. The number of neurons included in this analysis was 161 (20 deg/s), 159 (40 deg/s), and 139 (70 deg/s). (G) Same as D, but now for narrow spiking V1 neurons. The number of neurons included in this analysis was 67 (20 deg/s), 68 (40 deg/s), and 56 (70 deg/s).

direct and indirect pathways (i.e., direct feedback projections from AL and PM to V1, as well as pathways involving other cortical regions—in particular other HVAs—as well as cortico-thalamic loops).

An additional contrast between our and previous studies lies in the minor differences that we observed between the effect of inactivating AL and PM during wakefulness or isoflurane anesthesia. In spite of differences in speed preference between wakefulness and anesthesia (Fig. 1J), the effect of optogenetic inactivation of HVAs on V1 responses was very similar between the two brain states (see for instance Fig. 2 and Supplementary Fig. 5). Conversely, other studies reported that inactivation of HVAs more strongly affects V1 during wakefulness than anesthesia (Vangeneugden et al. 2019; Keller et al. 2020). This weaker effect of top-down modulation under anesthesia is in line with results from human subjects during loss of consciousness (Boly et al. 2011; Sikkens et al. 2019). A likely explanation for these different results lies again in the different type of stimulus that we used, which evokes less powerful activity changes in visual cortices compared with gratings.

Enhanced Sensory-Evoked Responses in V1 Come at the Expense of Orientation and Direction Selectivity

The enhancement of sensory-evoked responses that AL and PM induce in V1 comes, strikingly, at the expense of orientation and direction selectivity, both at the single-neuron and population level. This result is particularly surprising given the fact that the previous studies generally showed that HVAs enhance visual processing in V1. One study in particular (Pafundo et al. 2016) reported that inactivation of area LM decreased V1 responses to gratings moving along single neurons' preferred orientation and consequently also reduced orientation and direction selectivity of V1 neurons. In contrast, we observed a marked enhancement of orientation and direction tuning when AL and PM were inactivated (see the previous subsection for a discussion or possible reasons underlying the different results we observed). This finding suggests that the weaker orientation and direction tuning which is present in V1 with functionally intact AL and PM is likely sufficient to enable a proper processing of visual stimuli—although different results might have been obtained with other types of visual stimuli, such as moving gratings (e.g., Jin and Glickfeld 2020). Therefore, the visual system might operate in a regime that balances the processing of stimulus features such as orientation and direction with the ability to process stimuli which are smaller and (at least at the single-neuron level) less salient.

A second interpretation is that HVAs such as AL and PM might provide contextual, predictive representations to V1 via recurrent projections. Following a predictive processing framework (Rao and Ballard 1999; Friston 2005; Pennartz et al. 2019), higher order feedback may modulate V1 based on spatiotemporal predictions of sensory input, for example, modulating neuronal activity of V1 neurons whose receptive field lie along the expected trajectory of a moving object (Marques et al. 2018). Our findings that HVAs specifically modulate V1 responses during the rising phase of the response (as the moving bar enters their receptive field) are in line with this interpretation. This suggests that HVAs preferentially play a role in shaping the response of V1 neurons when sensory input is expected to hit their receptive field. Such HVA-mediated prediction-related enhancement in responses may be, from a functional point of view, more relevant than a further increase in orientation/direction selectivity. Moreover, this framework may explain why our results differ considerably from previous studies that used moving gratings, because the latter type of stimulus conveys a much higher spatial predictability across the visual field than an isolated moving bar.

Of relevance, the effects of AL and PM inactivation were similar on single-neuron orientation and direction tuning but different in terms of population decoding: inactivating AL improved population decoding of stimulus direction more than inactivation of PM did (Fig. 5). Recent studies also identified different functions of AL and PM in orientation discrimination and spatial integration, with PM showing larger receptive fields than AL (Murgas et al. 2020) and no involvement (in contrast with AL) in orientation discrimination (Jin and Glickfeld 2020).

Finally, it is worthwhile to highlight that the increased orientation and direction selectivity that we reported following inactivation to AL and PM are unlikely to be a consequence of an "iceberg" effect, in which most responses are silenced with the exception of the strongest ones. Indeed, we observed a reduction in responses (but not a complete suppression) in all neuronal cohorts we analyzed, irrespective of response amplitude or orientation/direction selectivity (Supplementary Fig. 12).

Higher Order Visual Areas Enhance Stimulus Responsiveness in V1

The classical framework to interpret visual processing in the neocortex follows a hierarchical approach, in which each subsequent processing stage is tasked with processing more complex stimulus features (Felleman and Van Essen 1991; Riesenhuber and Poggio 1999). HVA properties seem to support this view, as some higher order visual processing is either directly dependent upon or facilitated by them (Khastkhodaei et al. 2016; Tafazoli et al. 2017; Matteucci et al. 2019; Pak et al. 2020). Nevertheless, recent studies have shown that some key features of early visual processing, at the stage of V1, are enabled by virtue of top-down modulation originating in HVAs (Vangeneugden et al. 2019; Keller et al. 2020). Our study supports this notion, by indicating that, beyond being involved in the development of response features such as surround suppression (Vangeneugden et al. 2019), complex receptive fields (Keller et al. 2020), and higher level representations (Pak et al. 2020),

feedback information from HVAs also contributes to basic properties of V1 such as responses to oriented bars. Our experiments showed that AL and PM enhance weak sensory-evoked V1 responses more than strong ones. This may be explained by an added level of nonspecific background excitation that HVAs could provide to V1 neurons. Such additional excitation might modify the supposedly sigmoid input–output transfer function of V1 neurons in a way that more strongly amplifies weak inputs compared with strong ones. Other mechanisms, such as nonlinearities intrinsic to the generation of action potentials, cannot however be excluded.

By enhancing stimulus responsiveness, in particular to nonpreferred and small, unexpected visual features, just entering single neurons' receptive fields, HVAs such as AL and PM might play a role akin to that fulfilled by inverse effectiveness in the context of multisensory cue integration (Stein and Stanford 2008; Meijer et al. 2019). Specifically, HVAs might enhance, in particular at the single-neuron level, the signal-to-noise ratio of sensory-evoked responses to stimuli that would not otherwise induce large responses (for instance nonpreferred directions of movement, or stimuli entering the receptive field). This may provide a behavioral advantage by enabling to more reliably process small, barely noticeable visual stimuli.

Conclusion

Higher order visual areas are key elements of the cortical network of visual processing, as they not only further analyze visual information coming from V1 but also modulate the activity of V1 itself. Here, we showed how two HVAs with different response properties similarly enhance responses of V1, especially weak and unexpected ones (such as responses to nonpreferred directions, or responses to bars entering a neuron's receptive field). At the population level, AL and PM activity makes it easier for V1 to respond to moving bars but, at the same time, more difficult to decode their precise orientation and direction. Areas AL and PM therefore provide a major contribution to sculpting of V1 responses to simple visual objects: they effectively contribute to generating stronger and less sparse responses which, in turn, might make sensory-evoked responses to small, local, and possibly unexpected stimuli such as moving bars more robust and ultimately more reliable.

Supplementary Material

Supplementary material can be found at *Cerebral Cortex* online.

Funding

Notes

References

Andermann ML, Kerlin AM, Roumis DK, Glickfeld LL, Reid RC. 2011. Functional specialization of mouse higher visual cortical areas. *Neuron*. 72:1025–1039.

Berezovskii VK, Nassi JJ, Born RT. 2011. Segregation of feedforward and feedback projections in mouse visual cortex. *J Comp Neurol*. 519:3672–3683.

Boly M, Garrido MI, Gosseries O, Bruno M-A, Boveroux P, Schnakers C, Massimini M, Litvak V, Laureys S, Friston K. 2011. Preserved feedforward but impaired top-down processes in the vegetative state. *Science*. 332:858–862.

Cai L, Wu B, Ji S. 2018. Neuronal activities in the mouse visual cortex predict patterns of sensory stimuli. *Neuroinformatics*. 16:473–488.

Cossell L, Iacaruso MF, Muir DR, Houlton R, Sader EN, Ko H, Hofer SB, Mrsic-Flogel TD. 2015. Functional organization of excitatory synaptic strength in primary visual cortex. *Nature*. 518:399–403.

D'Souza RD, Bista P, Meier AM, Ji W, Burkhalter A. 2019. Spatial clustering of inhibition in mouse primary visual cortex. *Neuron*. 104:588–600.e5.

Erlich JC, Brunton BW, Duan CA, Hanks TD, Brody CD. 2015. Distinct effects of prefrontal and parietal cortex inactivations on an accumulation of evidence task in the rat. *Elife*. 4:e05457.

Felleman DJ, Van Essen DC. 1991. Distributed hierarchical processing in the primate cerebral cortex. *Cereb Cortex*. 1:1–47.

Ferguson KA, Cardin JA. 2020. Mechanisms underlying gain modulation in the cortex. *Nat Rev Neurosci*. 21:80–92.

Friston K. 2005. A theory of cortical responses. *Philos Trans R Soc Lond B Biol Sci*. 360:815–836.

Glickfeld LL, Andermann ML, Bonin V, Reid RC. 2013. Cortico-cortical projections in mouse visual cortex are functionally target specific. *Nat Neurosci*. 16:219–226.

Glickfeld LL, Olsen SR. 2017. Higher-order areas of the mouse visual cortex. *Annu Rev Vis Sci*. 3:251–273.

Glickfeld LL, Reid RC, Andermann ML. 2014. A mouse model of higher visual cortical function. *Curr Opin Neurobiol*. 24:28–33.

Goltstein PM, Montijn JS, Pennartz CMA. 2015. Effects of isoflurane anesthesia on ensemble patterns of Ca2+ activity in mouse v1: reduced direction selectivity independent of increased correlations in cellular activity. *PLoS One*. 10:e0118277.

Hanks TD, Kopec CD, Brunton BW, Duan CA, Erlich JC, Brody CD. 2015. Distinct relationships of parietal and prefrontal cortices to evidence accumulation. *Nature*. 520:220–223.

Harvey CD, Coen P, Tank DW. 2012. Choice-specific sequences in parietal cortex during a virtual-navigation decision task. *Nature*. 484:62–68.

Huh CYL, Peach JP, Bennett C, Vega RM, Hestrin S. 2018. Feature-specific organization of feedback pathways in mouse visual cortex. *Curr Biol*. 28:114–120.e5.

Ibrahim LA, Mesik L, Ji X-Y, Fang Q, Li H-F, Li Y-T, Zingg B, Zhang LI, Tao HW. 2016. Cross-modality sharpening of visual cortical processing through Layer-1-mediated inhibition and disinhibition. *Neuron*. 89:1031–1045.

Ji W, Gămănuț R, Bista P, D'Souza RD, Wang Q, Burkhalter A. 2015. Modularity in the Organization of Mouse Primary Visual Cortex. *Neuron*. 87:632–643.

Jin M, Glickfeld LL. 2020. Mouse higher visual areas provide both distributed and specialized contributions to visually guided behaviors. *Current Biology*. 30:4682–4692.

Keller AJ, Roth MM, Scanziani M. 2020. Feedback generates a second receptive field in neurons of the visual cortex. *Nature*. 582: 545–549.

Khastkhodaei Z, Jurjut O, Katzner S, Busse L. 2016. Mice can use second-order, contrast-modulated stimuli to guide visual perception. *J Neurosci*. 36:4457–4469.

Kim M-H, Znamenskiy P, Iacaruso MF, Mrsic-Flogel TD. 2018. Segregated subnetworks of Intracortical projection neurons in primary visual cortex. *Neuron*. 100:1313–1321.e6.

Ko H, Hofer SB, Pichler B, Buchanan KA, Sjöström PJ, Mrsic-Flogel TD. 2011. Functional specificity of local synaptic connections in neocortical networks. *Nature*. 473:87–91.

Korthauer K, Kimes PK, Duvallet C, Reyes A, Subramanian A, Teng M, Shukla C, Alm EJ, Hicks SC. 2019. A practical guide to methods controlling false discoveries in computational biology. *Genome Biol*. 20:118.

Krumin M, Lee JJ, Harris KD, Carandini M. 2018. Decision and navigation in mouse parietal cortex. *Elife*. 7:e42583.

Lamme VA, Zipser K, Spekreijse H. 1998. Figure-ground activity in primary visual cortex is suppressed by anesthesia. *Proc Natl Acad Sci U S A*. 95:3263–3268.

Licata AM, Kaufman MT, Raposo D, Ryan MB, Sheppard JP, Churchland AK. 2017. Posterior parietal cortex guides visual decisions in rats. *J Neurosci*. 37:4954–4966.

Madisen L, Mao T, Koch H, Zhuo J, Berenyi A, Fujisawa S, Hsu Y-WA, Garcia AJ 3rd, Gu X, Zanella S, et al. 2012. A toolbox of Cre-dependent optogenetic transgenic mice for light-induced activation and silencing. *Nat Neurosci*. 15:793–802.

Makino H, Komiyama T. 2015. Learning enhances the relative impact of top-down processing in the visual cortex. *Nat Neurosci*. 18: 1116–1122.

Mariño J, Schummers J, Lyon DC, Schwabe L, Beck O, Wiesing P, Obermayer K, Sur M. 2005. Invariant computations in local cortical networks with balanced excitation and inhibition. *Nat Neurosci*. 8:194–201.

Marques T, Nguyen J, Fioreze G, Petreanu L. 2018. The functional organization of cortical feedback inputs to primary visual cortex. *Nat Neurosci*. 21:757–764.

Marshel JH, Garrett ME, Nauhaus I, Callaway EM. 2011. Functional specialization of seven mouse visual cortical areas. *Neuron*. 72: 1040–1054.

Matteucci G, Bellacosa Marotti R, Riggi M, Rosselli FB, Zoccolan D. 2019. Nonlinear processing of shape information in rat lateral Extrastriate cortex. *J Neurosci*. 39:1649–1670.

Meijer GT, Marchesi P, Mejias JF, Montijn JS, Lansink CS, Pennartz CMA. 2020. Neural correlates of multisensory detection behavior: comparison of primary and higher-order visual cortex. *Cell Rep*. 31:107636.

Meijer GT, Mertens PEC, Pennartz CMA, Olcese U, Lansink CS. 2019. The circuit architecture of cortical multisensory processing: distinct functions jointly operating within a common anatomical network. *Prog Neurobiol*. 174:1–15.

Murgas KA, Wilson AM, Michael V, Glickfeld LL. 2020. Unique spatial integration in mouse primary visual cortex and higher visual areas. *J Neurosci*. 40:1862–1873.

Nassi JJ, Lomber SG, Born RT. 2013. Corticocortical feedback contributes to surround suppression in V1 of the alert primate. *J Neurosci*. 33:8504–8517.

Niell CM, Stryker MP. 2008. Highly selective receptive fields in mouse visual cortex. *J Neurosci*. 28:7520–7536.

Nurminen L, Merlin S, Bijanzadeh M, Federer F, Angelucci A. 2018. Top-down feedback controls spatial summation and response amplitude in primate visual cortex. *Nat Commun*. 9: 1–13.

Olcese U, Bos JJ, Vinck M, Lankelma JV, van Mourik-Donga LB, Schlumm F, Pennartz CMA. 2016. Spike-based functional connectivity in cerebral cortex and hippocampus: loss of global connectivity is coupled to preservation of local connectivity during non-REM sleep. *J Neurosci*. 36:7676–7692.

Olcese U, Iurilli G, Medini P. 2013. Cellular and synaptic architecture of multisensory integration in the mouse neocortex. *Neuron*. 79: 579–593.

Olcese U, Oude Lohuis M, Pennartz C. 2018. Sensory processing across conscious and nonconscious brain states: from single neurons to distributed networks for inferential representation. *Front Syst Neurosci*. 12:49.

Pafundo DE, Nicholas MA, Zhang R, Kuhlman SJ. 2016. Top-down-mediated facilitation in the visual cortex is gated by subcortical neuromodulation. *J Neurosci*. 36:2904–2914.

Pak A, Ryu E, Li C, Chubykin AA. 2020. Top-down feedback controls the cortical representation of illusory contours in mouse primary visual cortex. *J Neurosci*. 40:648–660.

Pennartz CMA, Dora S, Muckli L, Lorteije JAM. 2019. Towards a unified view on pathways and functions of neural recurrent processing. *Trends Neurosci*. 42:589–603.

Rao RPN, Ballard DH. 1999. Predictive coding in the visual cortex: a functional interpretation of some extra-classical receptive-field effects. *Nat Neurosci*. 2:79–87.

Raposo D, Kaufman MT, Churchland AK. 2014. A category-free neural population supports evolving demands during decision-making. *Nat Neurosci*. 17:1784–1792.

Riesenhuber M, Poggio T. 1999. Hierarchical models of object recognition in cortex. *Nat Neurosci*. 2:1019–1025.

Ringach DL, Shapley RM, Hawken MJ. 2002. Orientation selectivity in macaque V1: diversity and laminar dependence. *J Neurosci*. 22: 5639–5651.

Rossant C, Kadir SN, Goodman DFM, Schulman J, Hunter MLD, Saleem AB, Grosmark A, Belluscio M, Denfield GH, Ecker AS, et al. 2016. Spike sorting for large, dense electrode arrays. *Nat Neurosci*. 19:634–641.

Schmitzer-Torbert N, Jackson J, Henze D, Harris K, Redish AD. 2005. Quantitative measures of cluster quality for use in extracellular recordings. *Neuroscience*. 131:1–11.

Schnabel UH, Bossens C, Lorteije JAM, Self MW, Op de Beeck H, Roelfsema PR. 2018. Figure-ground perception in the awake mouse and neuronal activity elicited by figure-ground stimuli in primary visual cortex. *Sci Rep*. 8:1–14.

Sikkens T, Bosman CA, Olcese U. 2019. The role of top-down modulation in shaping sensory processing across brain states: implications for consciousness. *Front Syst Neurosci*. 13:31.

Song Y-H, Kim J-H, Jeong H-W, Choi I, Jeong D, Kim K, Lee S-H. 2017. A neural circuit for auditory dominance over visual perception. *Neuron*. 93:940–954.e6.

Stein BE, Stanford TR. 2008. Multisensory integration: current issues from the perspective of the single neuron. *Nat Rev Neurosci.* 9: 255–266.

Tafazoli S, Safaai H, De Franceschi G, Rosselli FB, Vanzella W, Riggi M, Buffolo F, Panzeri S, Zoccolan D. 2017. Emergence of transformation-tolerant representations of visual objects in rat lateral extrastriate cortex. *Elife.* 6:e22794.

Vaknin G, DiScenna PG, Teyler TJ. 1988. A method for calculating current source density (CSD) analysis without resorting to recording sites outside the sampling volume. *J Neurosci Methods.* 24: 131–135.

Vangeneugden J, van Beest EH, Cohen MX, Lorteije JAM, Mukherjee S, Kirchberger L, Montijn JS, Thamizharasu P, Camillo D, Levelt CN, et al. 2019. Activity in lateral visual areas contributes to surround suppression in awake mouse V1. *Curr Biol.* 29: 4268–4275.e7.

Vinck M, Bos JJ, Van Mourik-Donga LA, Oplaat KT, Klein GA, Jackson JC, Gentet LJ, Pennartz CMA. 2015. Cell-type and state-dependent synchronization among rodent somatosensory, visual, Perirhinal cortex, and hippocampus CA1. *Front Syst Neurosci.* 9:187.

Wang Q, Burkhalter A. 2007. Area map of mouse visual cortex. *J Comp Neurol.* 502:339–357.

Wang Q, Sporns O, Burkhalter A. 2012. Network analysis of corticocortical connections reveals ventral and dorsal processing streams in mouse visual cortex. *J Neurosci.* 32:4386–4399.

Wilson NR, Runyan CA, Wang FL, Sur M. 2012. Division and subtraction by distinct cortical inhibitory networks in vivo. *Nature.* 488: 343–348.